NUMERICAL STUDIES OF DROPLET BEHAVIOR IN A STEADY NON-UNIFORM ELECTRIC FIELD

A Thesis
Submitted to the Graduate Faculty
of the
North Dakota State University
of Agriculture and Applied Science

By

Ye Yao

In Partial Fulfillment of the Requirements
for the Degree of
MASTER OF SCIENCE

Major Department:
Mechanical Engineering

September 2013

Fargo, North Dakota

North Dakota State University

Graduate School

Title

Numerical Studies of Droplet Behavior in a Steady Non-Uniform Electric Field

By

Ye Yao

The Supervisory Committee certifies that this ***disquisition*** complies with North Dakota State University's regulations and meets the accepted standards for the degree of

MASTER OF SCIENCE

SUPERVISORY COMMITTEE:

Dr. Yechun Wang

Chair

Dr. Yildirim Bora Suzen

Dr. Iskander Akhatov

Dr. Benjamin Braaten

Approved:

11/8/2013 — Date

Dr. Alan R. Kallmeyer — Department Chair

ABSTRACT

An initially uncharged droplet suspended in another immiscible fluid under the influence of a steady non-uniform electric field may experience deformation, migration and bursting. This work numerically investigated the behavior of the droplet. Both the droplet and the suspending fluid are assumed as leaky-dielectric or perfect-dielectric. We used a three-dimensional spectral boundary element method which has been validated by comparing with other numerical results and experimental findings for droplet deformation in a uniform electric field. The electric properties of the fluids are found to have a big influence on the droplet migration direction and speed in a non-uniform electric field. We have investigated the droplet deformation and motion affected by permittivity ratio, resistivity ratio, viscosity ratio and the electric capillary number in a non-uniform electric field.

ACKNOWLEDGMENTS

First of all, I would like to thank my adviser Dr. Yechun Wang for her patient, kindly guidance and for giving me the opportunity to study and work under her supervision. I have benefitted a lot from her knowledge, experience and rigorous academic attitude.

I also want to thank Dr. Iskander Akhatov, Yildirim Bora Suzen and Dr. Benjamin Braaten for being honorable members of my defense committee. Your precious time and valuable suggestions helped me finish my research more efficiently.

I would like to thank Qixin Zhou and Xiaofeng Qu for their assistance during my studying and investigation.

I would also like to thank my dear parents, Youheng and Chunli, who always gave me my biggest support during my growing up.

This work is supported by National Science Foundation.

TABLE OF CONTENTS

LIST OF FIGURES

CHAPTER 1. INTRODUCTION

Since Taylor in 1934 [29] started to investigate electrohydrodynamics, the behavior of one liquid droplet that suspended in another immiscible fluid in an applied electric field has been developed in the last several decades. The initially uncharged droplet may experience deformation, migration and bursting, subjected to the combined action of electrical force, viscous force and surface tension. The electrical force tends to distort the droplet interface, while the surface tension tries to restore the original shape and viscous force slows down the action of two forces.

1.1. Applications

Apart from the basic research interest, electrohydrodynamics and dielectrophoresis have a huge potential for applications in emulsification [26], biophysics and bioengineering [10]. The applications for electrohydrodynamics include the deformation of a droplet in birefringence [21], atomization [24], enhancing the rate of mass or heat transfer between droplets and their surrounding fluids [11], enhancement of emulsion breaking, coalescence and demixing operations for dispersions [4]. The most significant application for dielectrophoresis is the dispersion of two different kinds of liquids. Dielectrophoresis could be useful for ink jet printing [23], biological separation of living and dead cells [6] and a variety processes involving multi-phase flows [5]. In recent years dielectrophoresis has been used for droplet generation and manipulation by digital microfluidics. Monodisperse droplets could be generated, combined, transported or separated according to the industry needs under the influence of an applied electric field [3].

1.2. Literature review

Under an applied electric field, the migration or the deformation, also called dielectrophoresis of the droplet, depends on the electric field type and the fluids properties (permittivies and resistivities). If the electric field supplies uniform electrical force, the droplet will only have deformation without migration. Early investigations focused on configurations that the droplet deforms into under the influence of uniform electric field

including electrohydrostatic(EHS) and electrohydrodynamics(EHD) [17]. For electrohydrostatic analysis, people assumed the suspended droplet and the surrounding fluid were perfect dielectrics. There are only normal electrical forces on the droplet surface and no tangential forces, so the droplet only deforms into a prolate shape. But since Taylor [28] started to consider both the droplet and the surround liquid to be slightly conductive (a leaky-dielectric system as referred to by his followers [1]), electrohydrodynamic theory has been employed by other researchers [1, 32, 11, 4], accounting to both tangential electrical force and normal electrical force. The oblate-like shape may be found in this situation.

Miksis [19] investigated theoretically and computationally the perfect dielectric system influenced by a uniform electric field. Assuming Stokes flow, integral equations were formulated for the problem, which was solved by a the boundary-element method (BEM). Sherwood [24] also used a BEM to compute a perfect-dielectric droplet deformation; Sherwood established models for the breakup of two droplets in a uniform electric field based on his experimental observations.

Feng and Scott [11] employed a Galerkin finite element method to investigate the leaky dielectric system under the uniform electric field created by parallel-plate electrodes. After that Feng used the same numerical method to investigate the droplet behavior in the range of finite electric Reynolds number. For droplets influenced by a uniform electric field, Lac and Homsy [17] predicted the droplet deformation and breakup via boundary integral method. Using a similar numerical method, Baygents, Rivette and Stone [4] investigated the motion and deformation of a pair of droplets in a uniform electric field. A finite volume/ front tracking method was used by Unverdi [33] and Fernandez [13, 12] to solve a similar problem. In addition, Hua, Lim and Wang [15] also used a finite volume/front tracking method to solve three different electric systems, including leaky dielectric system, perfect dielectric system and the droplet with constant surface charges. A coupled level-set and volume-of-fluid method was used to simulate droplet deformation in a uniform electric field [27]. This method has the advantage of automatic handling of topological changes. The disadvantages

of this method is that it can not inherently conserve mass [30]. Zhang and Kwok [37] developed a lattice Boltzmann method to compute the droplet behavior with the leaky dielectric theory under a uniform electric field.

Several studies conducted theoretical and experimental investigation utilizing the leaky dielectric theory to describe the droplet behavior under a uniform electric field. Allan and Mason [2] further developed Taylor's leaky dielectric theory and used a large number of liquid pairs in his experiments to validate the theoretical investigation. Vizika and Saville [34], Ha and Yang [14], Xu and Homsy [36] performed experiments to investigate the deformation of leaky dielectric droplets using parallel-plate electrodes. The transient theoretical analysis for the leaky dielectric droplet deformation under the uniform electric field was done by Zhang and Lin [16]. They solved a EHD deformation problem theoretically. Dubash and Mestel [9] also did the theoretical analysis for the transient droplet deformation, but their study focused on conducting inviscid droplet and solved a EHS deformation problem.

Few studies have focused on the droplet dynamics in a non-uniform electric field. Feng [10] theoretically analyzed the behavior of the droplet for a leaky dielectric system under a quadrapole electric field. His study predicted and compared the behavior of a droplet and a solid particle under the influence of the relative permittivities and conductivities in this type of electric field. A boundary integral method was employed to compute the droplet behavior under a similar electric field by Deshmukh and Thaokar [7]. Singh and Aubry [25] investigated the behavior and the interaction of a pair of droplets in a non-uniform electric field which was created by electrodes fixed on the bottom wall of a microfluidic device. Thaokar [31] combined a uniform electric field with a quadrapole component to supply non-uniform electrical force on droplets for a leaky dielectric system.

1.3. Objectives of this work

In our research, a three-dimensional spectral boundary element method was employed to investigate the droplet deformation and migration under a non-uniform electric field created by a point charge. We considered both a leaky dielectric system and a perfect

dielectric system in this work. This work is the foundation for future investigations on the droplet motion under an electric field created by co-planar electrodes, which could be found in digital microfluidics. The numerical method we used in this work combines the advantages of finite element method and boundary integral method. This method could also be used in the other computations involving interfacial dynamics.

We describe the mathematical formula and the boundary conditions in Chapter 2. The numerical scheme is introduced in Chapter 3. In Chapter 4 we validate the numerical scheme by comparing computational results with experimental findings and other numerical results. In Chapter 5, we present our computational results, including the droplet deformation and motion under the influence of fluid electric properties and electric field for leaky dielectric system under a non-uniform electric field. In Chapter 6, a droplet in a perfect dielectric system under a non-uniform electric field will be discussed and compared. Finally, conclusions and future work will be summarized in Chapter 7.

CHAPTER 2. MATHEMATICAL FORMULATION

2.1. Definition of the problem

In this research, we investigate the migration and the deformation of an initially uncharged neutrally buoyant droplet suspended in another immiscible liquid. A steady non-uniform electric field is applied. We assume both the surrounding fluid and the suspended droplet are Newtonian and incompressible. The behavior of the droplet is governed by the continuity and Stokes equations. In this section we define the problem and summarize the basic equations for electrohydrodynamic investigation assuming a leaky dielectric system or a perfect dielectric system.

The problem could be illustrated in Fig. 1. The electric field intensity is denoted as $\boldsymbol{E}^{\infty}$. The droplet (Fluid 1) possesses a resistivity of $R\chi$, permittivity of $Q\varepsilon$ and viscosity of $\lambda\mu$, while the suspending fluid (Fluid 2) has a resistivity of χ, permittivity ε and viscosity μ. The surface tension of the interface between the two fluids is denoted as γ.

In this study, the droplet behavior is affected by electrical stress and surface tension. A dimensionless number, electric capillary number Ca_E is employed in this study.

$$Ca_E = \frac{a\varepsilon\varepsilon_0(E^{\infty})^2}{\gamma} \tag{1}$$

where a is the radius of the initially undeformed droplet and is used as the length scale of the problem. ε is the relative permittivity of the fluid outside the droplet and ε_0 is that of the vacuum. E^{∞} is the magnitude of the electric field intensity $\boldsymbol{E}^{\infty}$.

Several important dimensionless parameters are used. All lengths in our work are scaled with a, velocity with $a\varepsilon\varepsilon_0(E^{\infty})^2/\mu$ and time with $\mu/\varepsilon\varepsilon_0(E^{\infty})^2$.

2.2. Boundary integral equation and electrical forces

When the Reynolds number is sufficiently small, the inertial terms in the Navier-Stokes

could be neglected. The governing equations for fluids are,

$$\nabla \cdot \boldsymbol{\sigma} = -\nabla p + c\nabla^2 \boldsymbol{u} = \mathbf{0} \tag{2}$$

$$\nabla \cdot \boldsymbol{u} = 0 \tag{3}$$

where $c = \mu$ for the surrounding fluid and $c = \lambda\mu$ for the depositing fluid. The boundary conditions on the drop interface Γ include,

$$\boldsymbol{u} = \boldsymbol{u}_1 = \boldsymbol{u}_2 \tag{4}$$

In this study, a point charge is used to supply a non-uniform electric field as shown in Fig. 2, $\boldsymbol{E}^{\infty}$ is a function of the distance to the point charge q, which is located at the origin of the coordinate system,

$$\boldsymbol{E}^{\infty} = \frac{q\boldsymbol{r}}{4\pi\varepsilon\varepsilon_0|\boldsymbol{r}|^3} \tag{5}$$

where $\boldsymbol{r} = (x, y, z)$. The electric capillary number Ca_E is determined when the electric field intensity is at $|\boldsymbol{r}| = a$.

According to Gauss' law, the electric field inside and outside the droplet all satisfy,

$$\nabla \cdot \boldsymbol{E} = 0 \tag{6}$$

The magnitude of the electric field normal to the interface E_n may be obtained by solving the following boundary integral equation [4, 17]

$$\boldsymbol{E}^{\infty} \cdot \boldsymbol{n}(\boldsymbol{x_0}) + \frac{1-R}{4\pi} \int_{\Gamma} \frac{\boldsymbol{r} \cdot \boldsymbol{n}(\boldsymbol{x_0})}{|\boldsymbol{r}|^3} E_n(\boldsymbol{x}) dS = \frac{1+R}{2} E_n(\boldsymbol{x_0}) \tag{7}$$

where $\boldsymbol{r} = \boldsymbol{x}_0 - \boldsymbol{x}$. The tangential part of $\boldsymbol{E}$, $\boldsymbol{E}_t = \boldsymbol{E} - E_n\boldsymbol{n}$ can then be found by

$$\boldsymbol{E}_t = \boldsymbol{E}^\infty + \int_\Gamma \frac{\boldsymbol{r}}{4\pi|\boldsymbol{r}|^3}(1-R)E_n dS - \frac{1+R}{2}E_n\boldsymbol{n} \tag{8}$$

With E_n and $\boldsymbol{E}_t$ obtained, the jump of stress created by the discontinuity of the electric field for the leaky dielectric system can be calculated by

$$\Delta\boldsymbol{f}_E = \frac{1}{2}[(1-QR^2)E_n^2 - (1-Q)|\boldsymbol{E}_t|^2]\boldsymbol{n} + (1-RQ)E_n\boldsymbol{E}_t \tag{9}$$

And the jump of stress due to the discontinuity of the electric field for the perfect dielectric system could be gotten by

$$\Delta\boldsymbol{f}_E = \frac{1}{2}(E_n^2 + Q\boldsymbol{E}_t^2)(1-\frac{1}{Q})\boldsymbol{n} \tag{10}$$

The stress on the droplet surface could be expressed by

$$\Delta\boldsymbol{f} \equiv \boldsymbol{f}_2 - \boldsymbol{f}_1 = \frac{1}{Ca_E}(\nabla_S \cdot \boldsymbol{n})\boldsymbol{n} - \Delta\boldsymbol{f}_E \tag{11}$$

Where the subscripts "1" and "2" represent fluid inside and outside of the droplet respectively. The unit normal $\boldsymbol{n}$ is pointing towards the suspending fluid.

For a given droplet interface Γ, the velocity at an arbitrary point on the interface $\boldsymbol{x}_0$ may be determined by the boundary integral equation [22, 35, 8],

$$(1+\lambda)\boldsymbol{u}(\boldsymbol{x}_0) = -\frac{1}{4\pi\mu}\int_\Gamma \left[\boldsymbol{S}\cdot\Delta\boldsymbol{f} - (1-\lambda)\mu\boldsymbol{T}\cdot\boldsymbol{u}\cdot\boldsymbol{n}\right](\boldsymbol{x})dS \tag{12}$$

Kernel $\boldsymbol{S}$ is the fundamental solution for the Stokes equations and $\boldsymbol{T}$ is the associated stress.

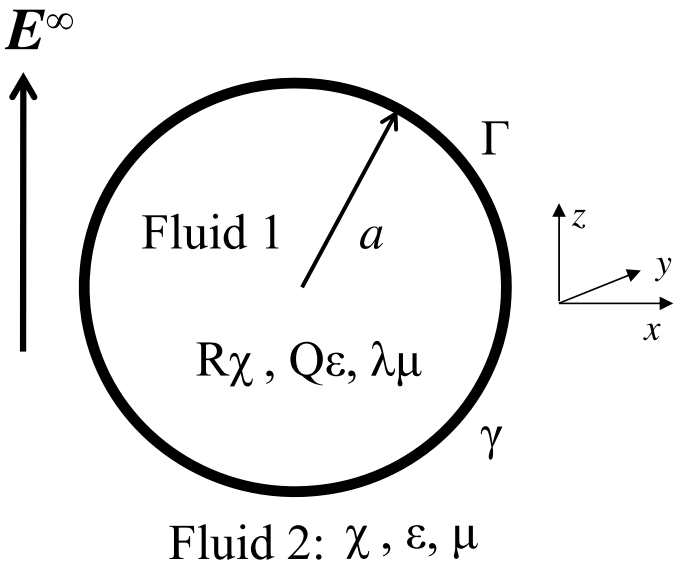

Figure 1. Schematic for a droplet in a uniform DC electric field E^{∞}.

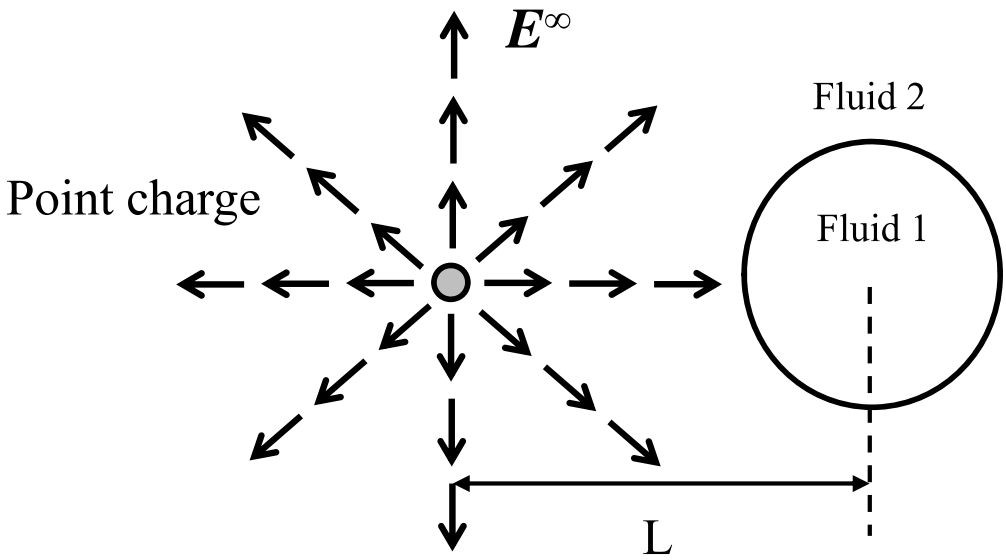

Figure 2. Schematic for a droplet in a non-uniform DC electric field E^{∞} created by a point charge.

CHAPTER 3. NUMERICAL METHOD

In this part we will briefly introduce our numerical method. The details of this method could be found in literatures[8, 35]. We use a three-dimensional spectral boundary element method for interfacial dynamics in Stokes flow to solve the aforementioned integral equations. It could be used to solve some complicated geometries with less denser systems and save a large amount of time.

3.1. Spectral boundary discretization

As shown in Fig. 3, we divided the droplet surface into a moderate number N_E (N_E=6 in our research) of curvilinear quadrilateral elements. This method is based on the spectral points defined on each element, so the calculations via interpolations are more efficient and accurate. The geometry and physical variables on each element are discretized via Lagrangian interpolation in terms of ξ and η on the square interval $[-1, 1]^2$ [35].

We use cube projection to discretize the initial spherical interface. There are two different types of points admitted by boundary integral equations (7) and (12). One is the collocation points $\boldsymbol{x}_0$ on the left side of the equations, which are used to hold the equations. Another type is the basis points $\boldsymbol{x}$ on the right side of the equations. They are where the physical variables $\boldsymbol{u}$ and $\boldsymbol{f}$ are solved or defined. Collocation points $\boldsymbol{x}_0$ of Legendre-Gauss quadrature and basis points $\boldsymbol{x}$ of Legendre-Gauss-Lobatto quadrature are employed in the three-dimensional spectral boundary method. Hence, singularity problems are avoided.

3.2. Explicit time-integration algorithm

To determine the droplet interfacial velocity $\boldsymbol{u}$, a fourth-order Runge-Kutta algorithm with a typical time step of 5×10^{-4} is used to update the Gauss-Lobatto basis points via the kinematic condition,

$$\frac{d\boldsymbol{x}}{dt} = (\boldsymbol{u} \cdot \boldsymbol{n})\boldsymbol{n} + U_t\boldsymbol{t} \tag{13}$$

where the first term on the right hand of the equation represents the normal interfacial velocity, $\boldsymbol{t}$ is the interfacial tangent unit and U_t is a parameter influenced by the droplet

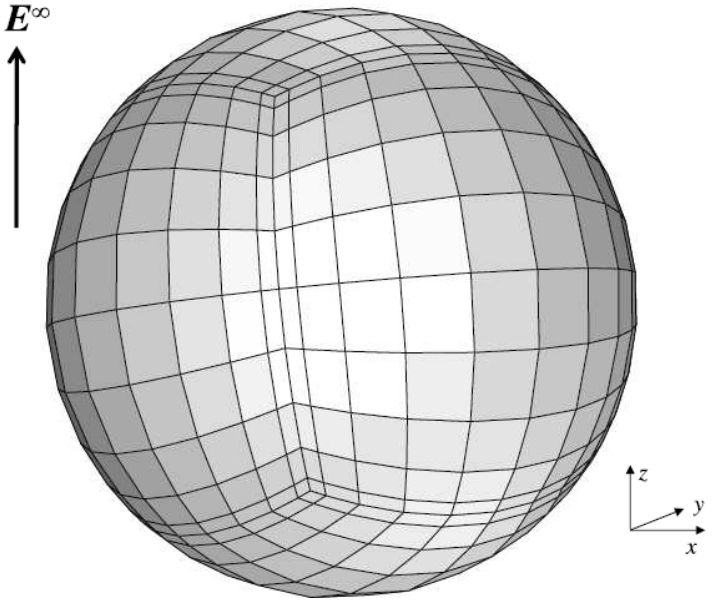

Figure 3. 3D droplet geometry in a uniform DC electric field E^∞.

centroid velocity and the tangent velocity on the droplet interface. U_t in this equation is used to adjust the distribution of the mesh spontaneously [20].

3.3. Convergent test

In order to determine the numbers of spectral points N_B to use in each curvilinear quadrilateral elements, we conducted convergent tests for the uniform electric field in Fig. 4 and for the non-uniform electric field in Fig. 5. For both of the figures, we keep the parameters R, Q, Ca_E and λ the same and consider the relative error in droplet deformation D as a function of a variety of N_B values. Deformation of a droplet D is defined in Chapter 4. The relative error in deformation D was obtained based on the value of N_B=15. We found good convergence when $N_B > 10$ for both of the uniform electric field and non-uniform electric field, and hence we used N_B=11 as the basis point in our research, which created a relative error of $O(10^{-3})$ in computations. There are $N_B \times N_B = 121$ spectral points in each spectral element. We also used $N_B = 10$ as the basis point in some computations.

We plot the relation between the relative error in D and the time step Δt for the

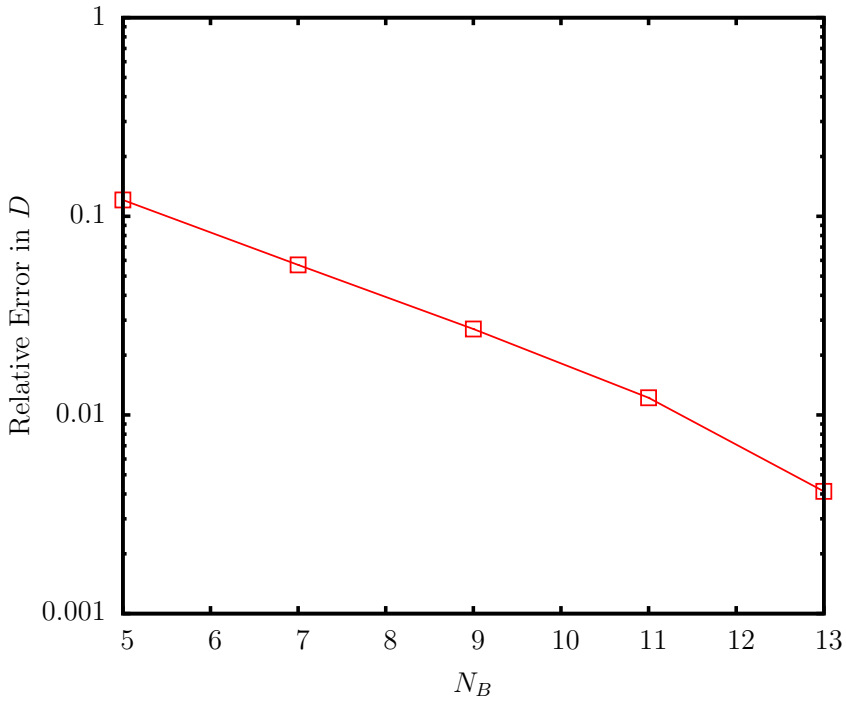

Figure 4. The relative error in droplet deformation D as a function of the number of spectral points N_B. Deformation is computed for a droplet influenced by a uniform electric field. $Ca_E = 0.2, R = 0.1, Q = 0.1$ and $\lambda = 1$.

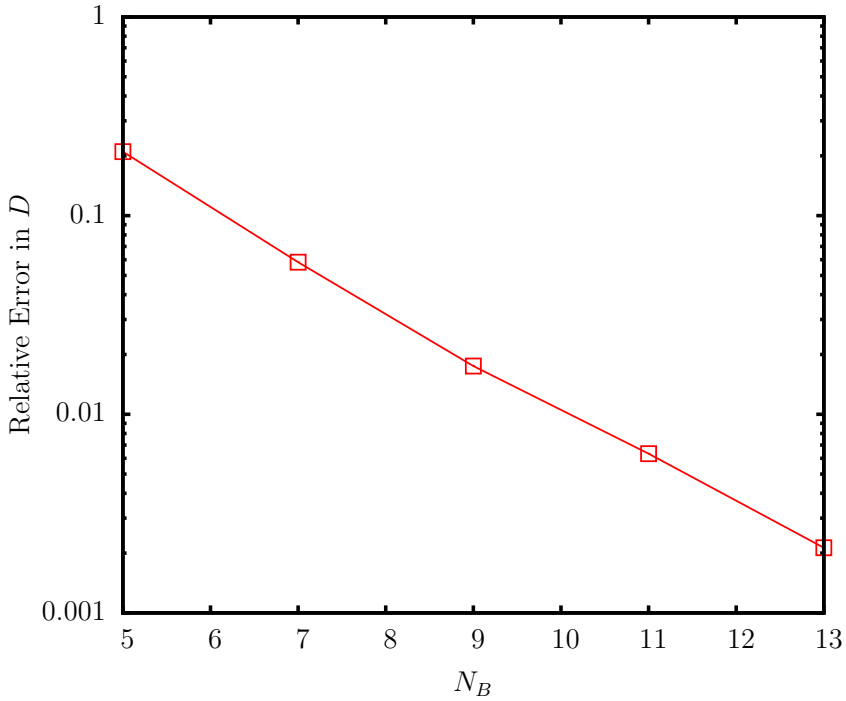

Figure 5. The relative error in droplet deformation D as a function of the number of spectral points N_B. Deformation is computed for a droplet influenced by a non-uniform electric field. $Ca_E = 0.2, R = 2, Q = 2, L = 1.5$ and $\lambda = 1$.

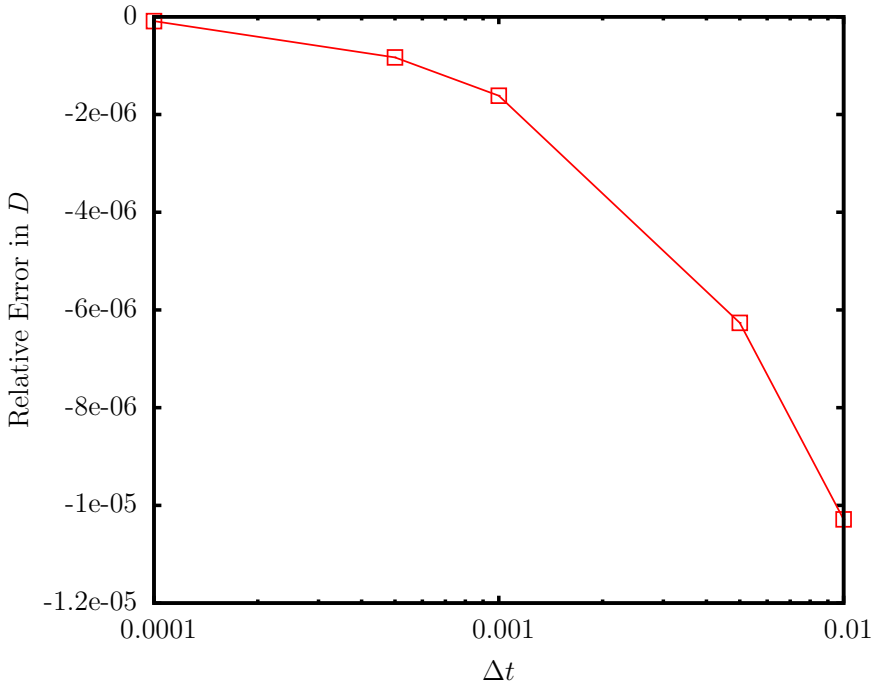

Figure 6. The relative error in droplet deformation D as a function of the time step Δt. Deformation is computed for a droplet influenced by a non-uniform electric field. $Ca_E = 0.2, R = 2, Q = 2, L = 1.5$ and $\lambda = 1$.

non-uniform electric field in Fig. 6. The relative error in deformation D was obtained based on D computed using $\Delta t = 1 \times 10^{-4}$. Good convergence for was found and $\Delta t = 5 \times 10^{-4}$ was employed in our computations of the droplet behaviors.

CHAPTER 4. VALIDATION

In order to validate our computational approach, we compare our numerical results which are generated by a uniform electric field with the theoretical predictions and experimental findings. From literature we could find that the electric properties of fluids, including resistivity ratio R and permittivity ratio Q, determine the droplet shape at steady state if stable. To make the comparison convenient, the droplet deformation is defined as,

$$D = \frac{l_z - l_x}{l_z + l_x} \tag{14}$$

As shown in Fig. 7, we define l_z as the droplet maximum length in direction of the electric field and l_x perpendicular to the electric field direction. When D is positive, the droplet deforms to a prolate shape, such as Fig. 8 (a); when D is negative, an oblate shape is formed, like Fig. 8 (b).

For validation, we use the same parameters with Lac and Homsy [17] to calculate the droplet deformation changing with different Ca_E as shown in Fig. 9. The dotted line shows the results of the small-deformation theory by Taylor in 1966 and the dashed asymptotic line comes from second order theory by Ajayi in 1978. But both of their theories are only accurate to predict small deformation of the droplet. So when the droplet deformation becomes larger and larger, the theoretical predictions of Taylor and Ajayi start to derive from others' results. Lac and Homsy [17], Deshmukh and Thaokar [7] have given detailed analysis on why first and second order theories are not accurate to predict larger droplet deformation. As shown in Fig. 9, for both cases (prolate and oblate shapes), our computational results show good agreements with Lac and Homsy's predictions.

Experiments have been carried out to validate our computations. A water droplet was suspended in castor oil under the influence of a uniform electric field in our experiment. The uniform electric field was generated by two copper plate electrodes with a size of 4 cm x 4 cm. A CCD camera (Allied Vision Technologies Canada Inc., Prosilica GC) with

microscopic lenses was employed to record the deformation of the droplet. We mounted the whole devices on the platform of FTA1000B goniometer (First Ten Angstroms Inc.). Using the pendant-droplet technique, we got the surface tension $\gamma = 17.6 \pm 0.68$ mN/m in room temperature. In order to compare with experimental data from Vizika and Saville [34], we use the same parameters: $Q = 17.54$, $R = 1/1500$, $\lambda = 1/1400$, and $\gamma = 16.8$ mN/m in our simulations. As shown in Fig. 10, when the droplet experiences a small or moderate deformation, our computational results agree well with experiments. Fig. 11 shows a good comparison in droplet shape between our computational result and experimental result. For large deformation, the mismatch with experiments may be due to the fact that we ignore the existence of parallel plate electrodes in the vicinity of the droplet in computations while the influence of the electrodes is significant in experiments for large deformations.

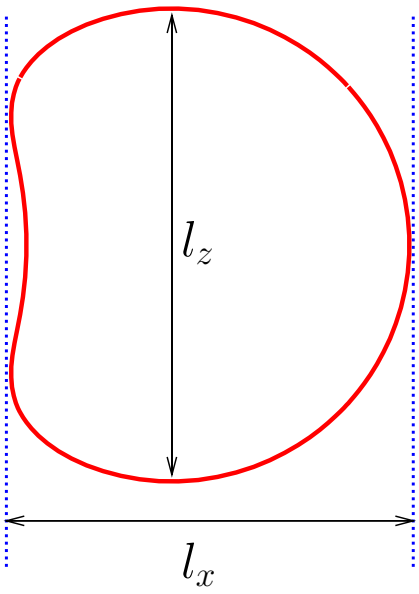

Figure 7. The measurement of l_x and l_z for a deformed droplet.

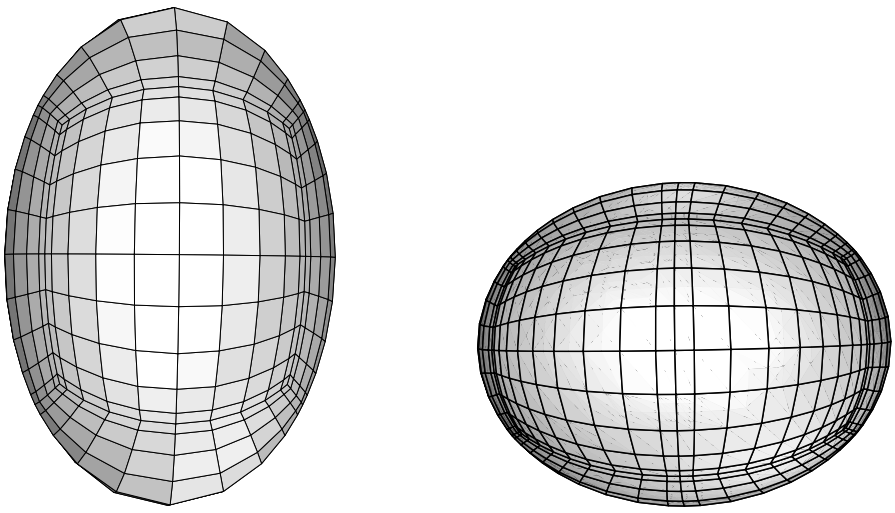

(a) (b)

Figure 8. (a) 3D shape of prolate. (b) 3D shape of oblate.

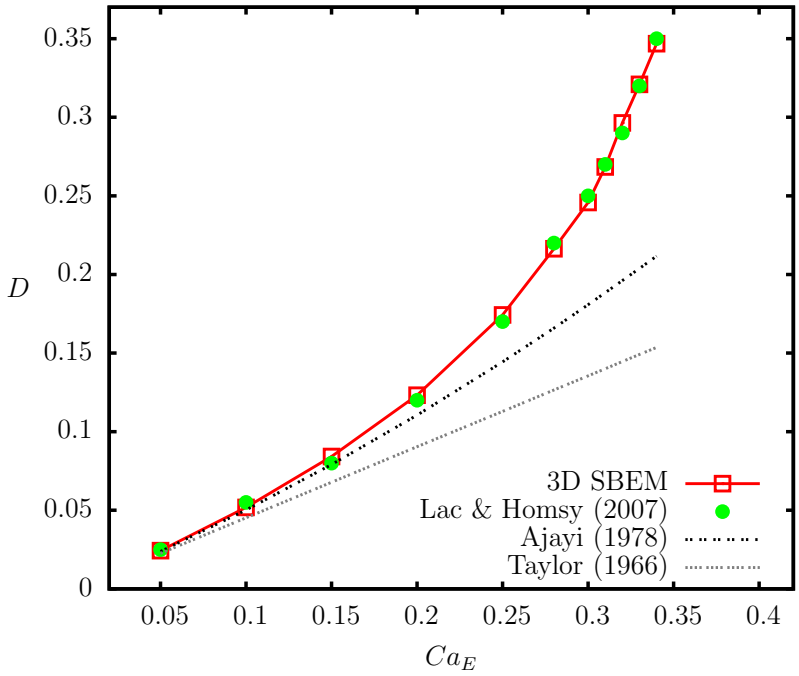

(a)

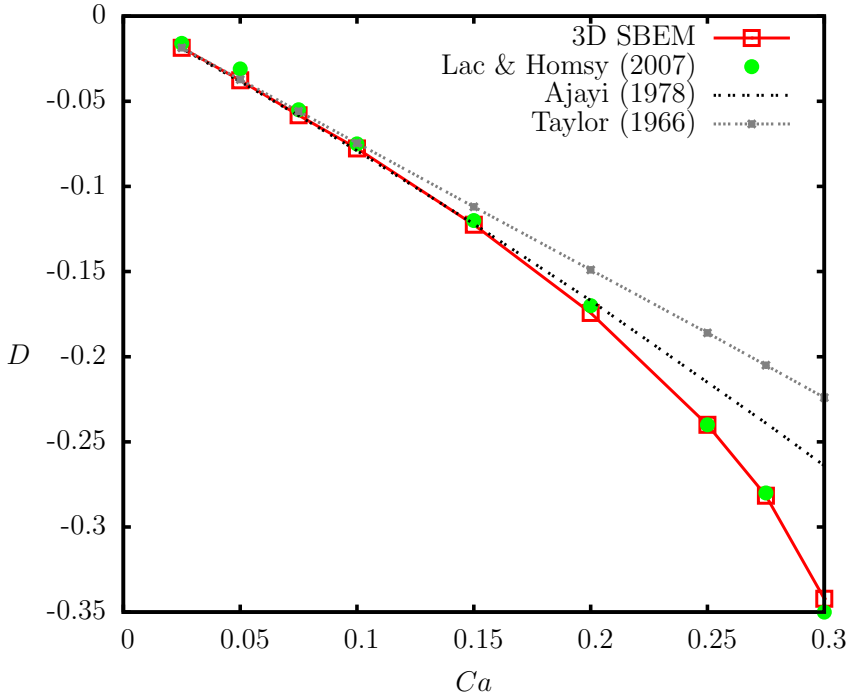

(b)

Figure 9. Comparison of our results with Lac and Homsy, Ajayi and Taylor under uniform electric field. (a) $R = 0.1$, $Q = 0.1$ and $\lambda = 1$. (b) $R = 10$, $Q = 2$ and $\lambda = 1$.

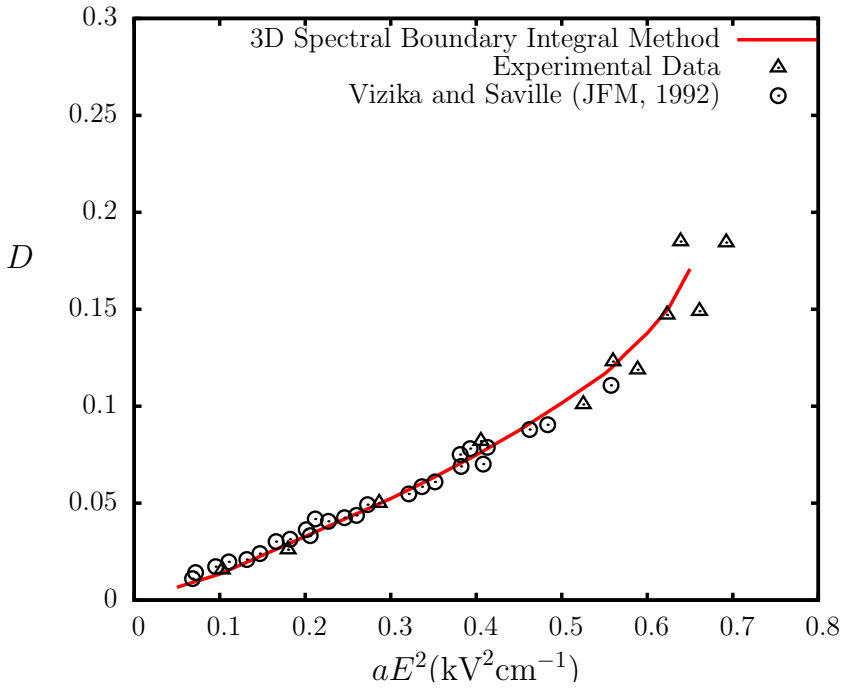

Figure 10. Steady-state deformation of a water droplet suspended in caster oil as a function of $a(E^\infty)^2$ ($kV^2\mathrm{cm}^{-1}$). Our spectral boundary element results, experimental data by Vizika & Saville [34] and our own measurements are included for comparison.

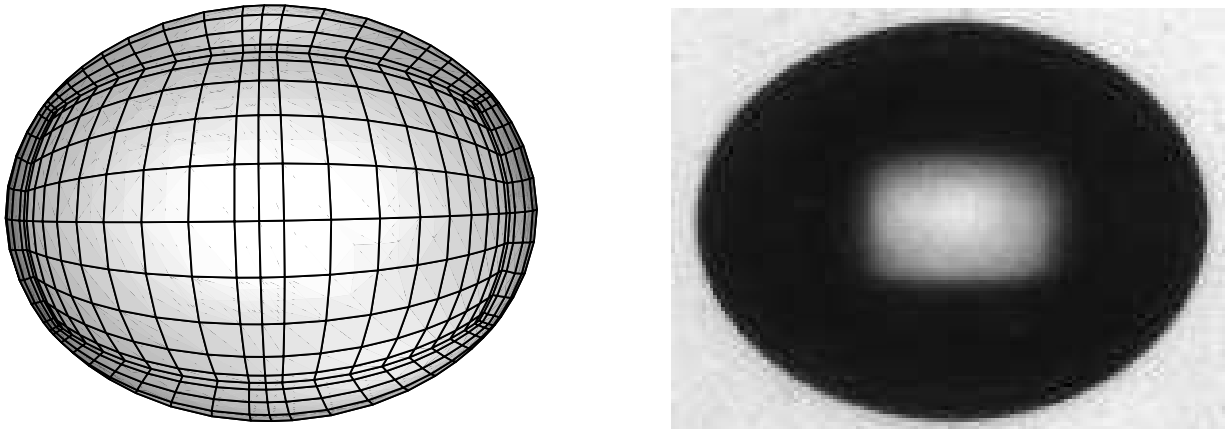

Figure 11. The steady-state shape of a water droplet suspended in caster oil for $a(E^\infty)^2 = 0.56kV^2\mathrm{cm}^{-1}$.

CHAPTER 5. BEHAVIOR OF A LEAKY DIELECTRIC DROPLET

Since Taylor [18] developed the leaky dielectric model, leaky dielectric model and perfect dielectric model have been investigated by several authors [19, 17, 10, 15] with different numerical methods. An ideal perfect dielectric has absolutely no conductivity, its resistivity is infinite. But the real dielectric liquids in this world are not perfect; most of them are leaky dielectric liquids. A leaky dielectric could be defined as a poorly conducting liquid, they just conduct a small amount of electrical current. From Maxwell's equations, the characteristic time for electric phenomena t_e is given by

$$t_e = \frac{\varepsilon}{\sigma} \tag{15}$$

where ε is the electric permittivity, and σ is the conductivity. The viscous time scale of the fluid motion t_v can be identified as:

$$t_v = \frac{\rho L^2}{\mu} \tag{16}$$

where ρ and μ are the density and viscosity of the fluid and L is the characteristic length scale. If both of the liquids are electrically conductive and satisfy the condition $t_e \ll t_v$, leaky dielectric model could be used. Free charges would accumulate on the interface of the droplet under an applied electric field. Not only normal direction stress, but also shear stress is produced and exerted on droplet interface. When two liquids system satisfy the condition $t_e \gg t_v$, fluids could be considered as perfect dielectrics. Perfect dielectric model is different from the other model, since there is no embedded charges. For perfect dielectrics, electrical stresses are perpendicular to the interface. The droplet deformation combined with the interfacial tension serves to balance the electric stress. In this thesis, both models will be discussed.

In this part, a point charge was employed to supply a steady non-uniform electric field,

and the point charge was located at the origin of a Cartesian coordinate system. As shown in Fig. 2, an initially spherical droplet suspended in another fluid is released at an initially position that has a distance L to the point charge. Due to the non-uniform electric field and the asymmetry of the problem, the droplet not only deforms, but also migrates. According to the electric properties of the fluids, the droplet may moves to the stronger electric field where the electric intensity is larger, or towards weaker field where the electric intensity is smaller. In this section, we will discuss how these parameters, including resistivity ratio R, permittivity ratio Q, electric capillary number Ca_E and viscosity ratio λ influence the droplet deformation and migration. As shown in Fig. 7, the definition of the droplet deformation D follows Eq. (14) in Chapter 4 although l_z is no longer in parallel with the electric field direction. Owning to symmetry with respect to x axis, the droplet only migrates in x direction. Therefore, we use u_x as the droplet centroid velocity in our research.

5.1. Influence of electric properties of fluids

5.1.1. Droplet velocity

Permittivity ratio Q and resistivity ratio R are found to have a significant affect to the droplet migration velocity. Fig. 12 explains the initial centroid velocity of the droplet at time t=0 changes with R and Q. Other parameters Ca_E, λ and L are kept constant. When the droplet moves towards the point charge, the droplet centroid velocity u_x is defined as negative. when the droplet moves away from the point charge to the weaker electric field u_x is positive. From this figure we could find that when $R > 1$ (the droplet is more resistive than the suspending fluid), the droplet always migrates away from the point charge; while the droplet always migrates to the stronger electric field if $R < 1$. If $R = 1$, the direction of the droplet movement is determined by Q. In this case, when the droplet has less polarizability than the surrounding fluid ($Q < 1$), u_x will be positive; when $Q > 1$ the droplet then moves towards the point charge and u_x is negative. Fig. 13 and Fig. 14 explain the influence of resistivity ratio R on velocity as the droplet migrates. Q, Ca_E and λ are the same for both of the figures. When $R < 1$, u_x is negative and the droplet moves faster with a smaller R.

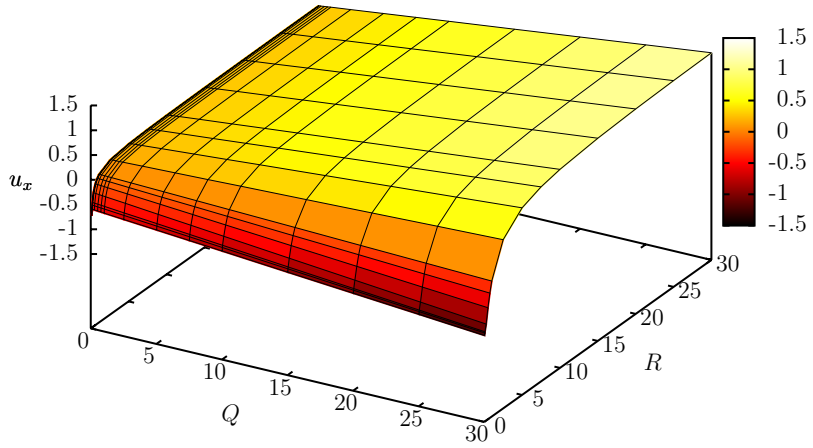

Figure 12. Initial droplet velocity u_x as a function of the permittivity ratio Q and the resistivity ratio R for a droplet with $Ca_E = 0.2$, $\lambda = 1$ and $L = 1.5$.

On the contrary, u_x will be positive if $R > 1$ and the droplet migrates faster with a larger R, as shown in Fig. 14. The droplet velocity decreases when the droplet moves to the weaker electric field.

For $R = 1$, the droplet migration direction is determined by Q. In the case of $Q < 1$, as shown in Fig. 15, the droplet migrates to the further position from the point charge. The droplet is found to travel faster with a smaller Q value when $Q < 1$. The velocity magnitude dramatically increases when the droplet is released initially. The velocity reaches the maximum value soon after the droplet starts to move and then decreases slowly. In Fig. 16, all parameters are identical with Fig. 15 except for Q. For $Q > 1$ the droplet is released at the distance $L = 1.5$, it migrates towards the point charge. The velocity magnitude suddenly decreases at the beginning and then tends to maintain the same value. A larger velocity value could be observed for larger Q in this case. Fig. 17 shows the droplet centroid location x_c as a function of time t under the influence of Q when $R = 1$. From this figure we find that when both liquids' resistivity are the same the larger difference in permittivity the two liquids have, the higher migration speed the droplet obtains.

But when R is not equal to 1, the conclusion is different. No matter what direction the droplet migrates, a larger Q value will lead to a faster migration speed as shown in Fig. 18 and Fig. 19.

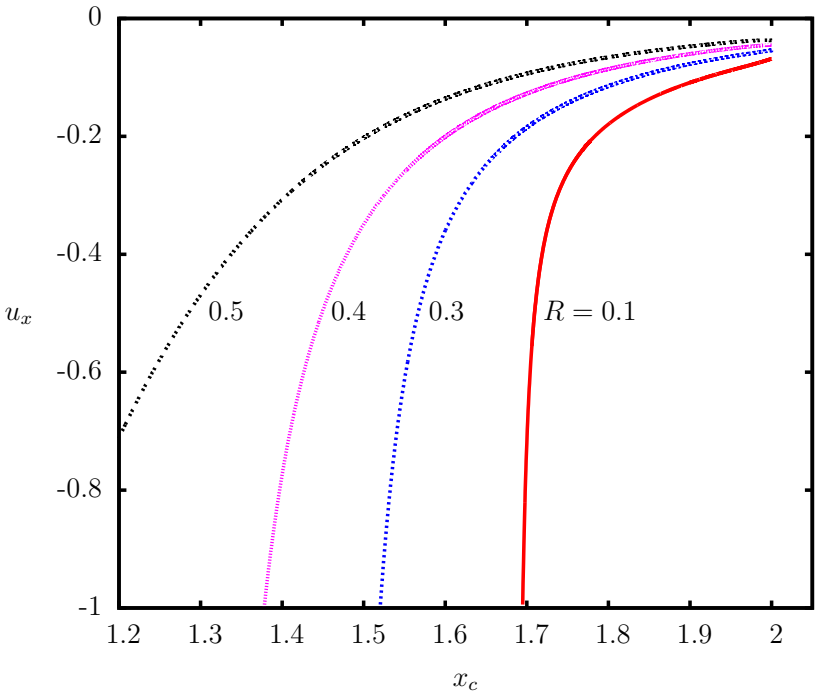

Figure 13. Droplet velocity u_x as a function of location x_c under the influence of R. $Ca_E = 0.2$, $Q = 10$, $R < 1$, $L = 2$ and $\lambda = 1$.

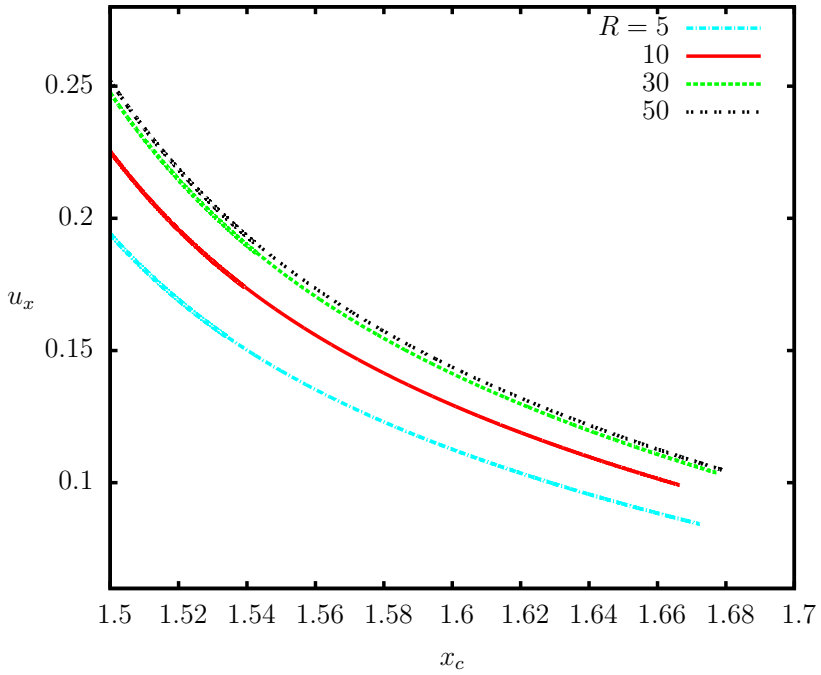

Figure 14. Droplet velocity u_x as a function of location x_c under the influence of R. $Ca_E = 0.2$, $Q = 10$, $R > 1$, $L = 2$ and $\lambda = 1$.

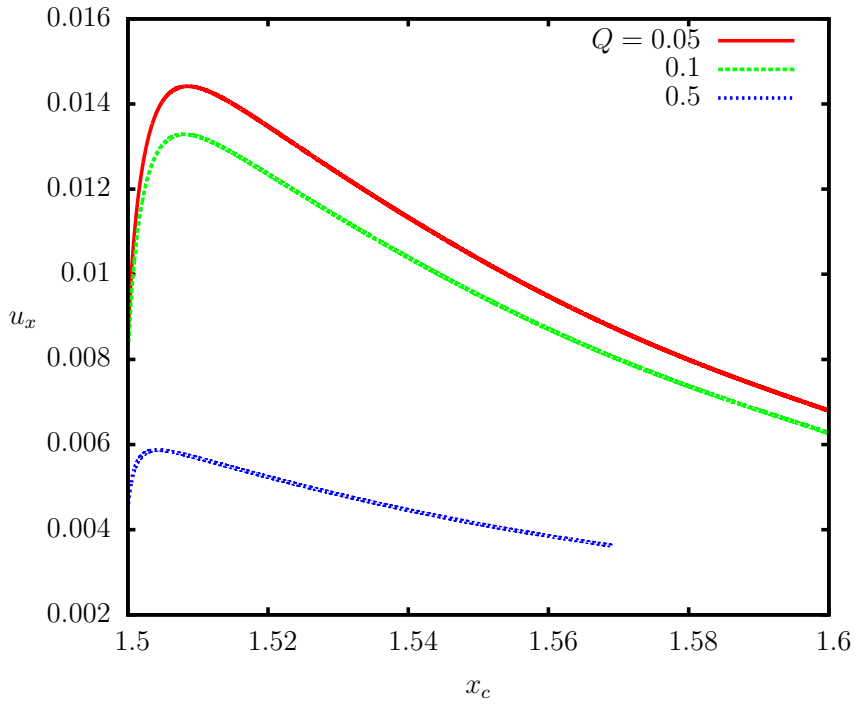

Figure 15. Droplet velocity u_x as a function of location x_c under the influence of Q when $Ca_E = 0.2$, $R = 1$, $Q > 1$, $L = 1.5$ and $\lambda = 1$.

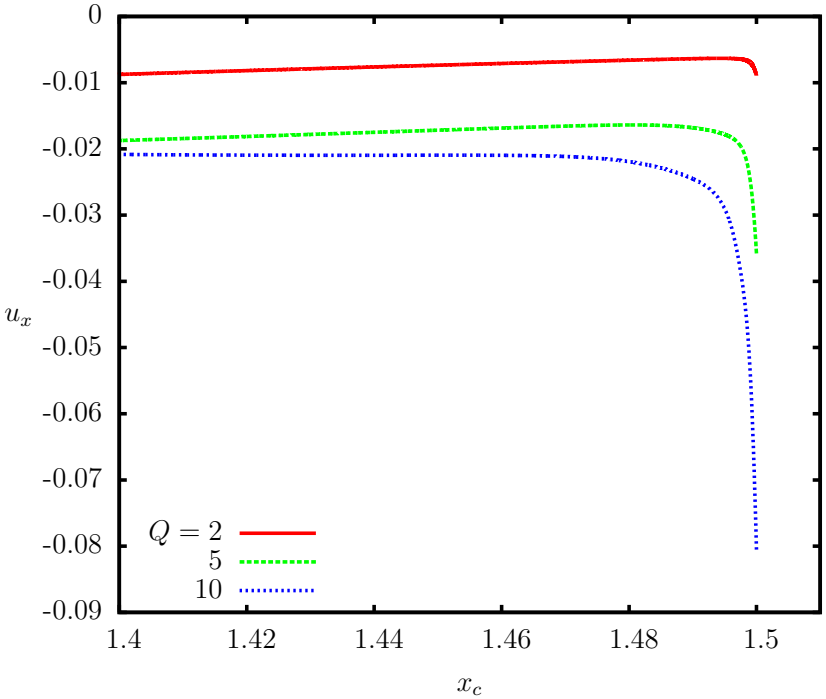

Figure 16. Droplet velocity u_x as a function of location x_c under the influence of Q when $Ca_E = 0.2$, $R = 1$, $Q > 1$, $L = 1.5$ and $\lambda = 1$.

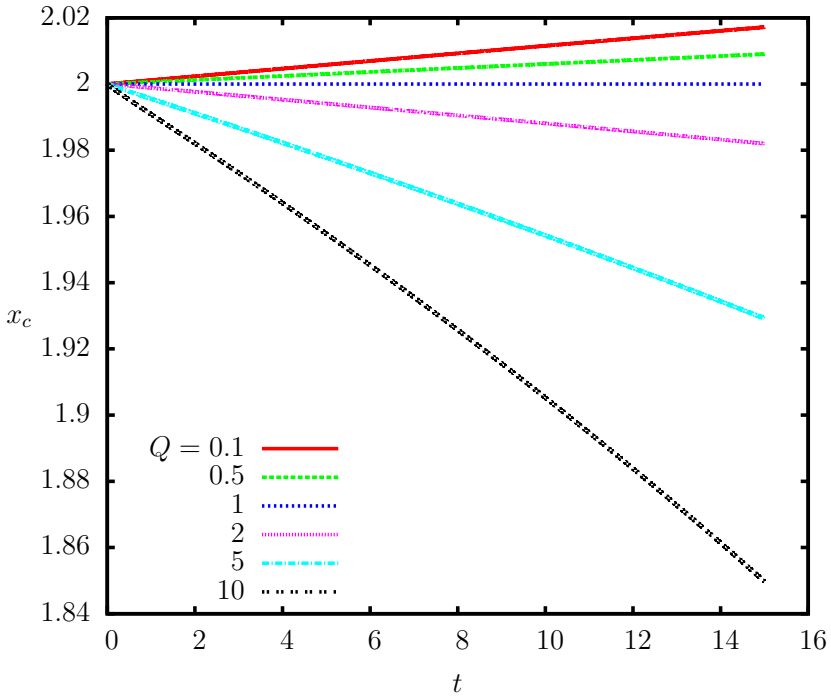

Figure 17. Droplet centroid location x_c as a function of time t under the influence of Q when $Ca_E = 0.2$, $R = 1$, $L = 2$ and $\lambda = 1$.

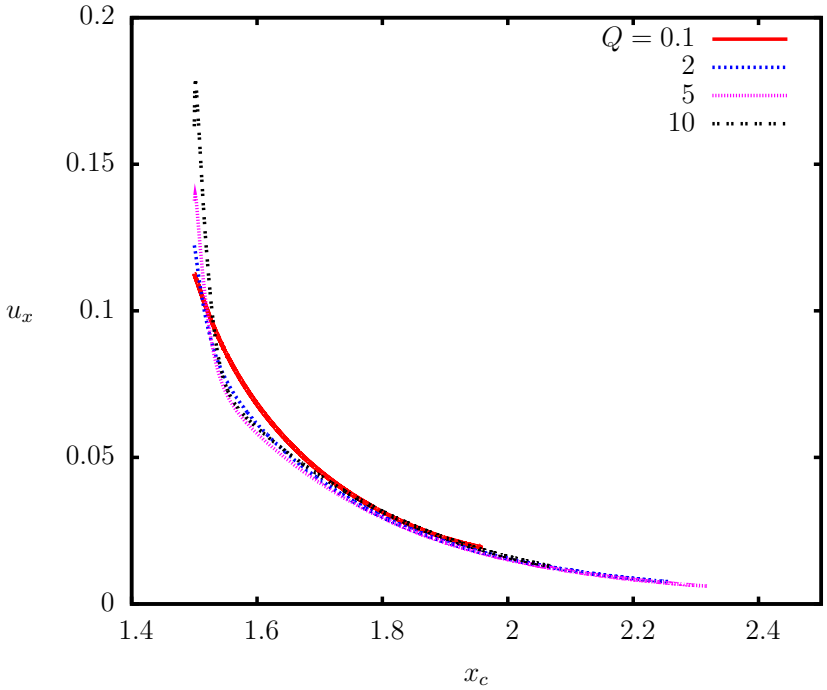

Figure 18. Droplet centroid velocity u_x as a function of location x_c under the influence of Q. $R = 2$, $Ca_E = 0.2$, $L = 1.5$ and $\lambda = 1$.

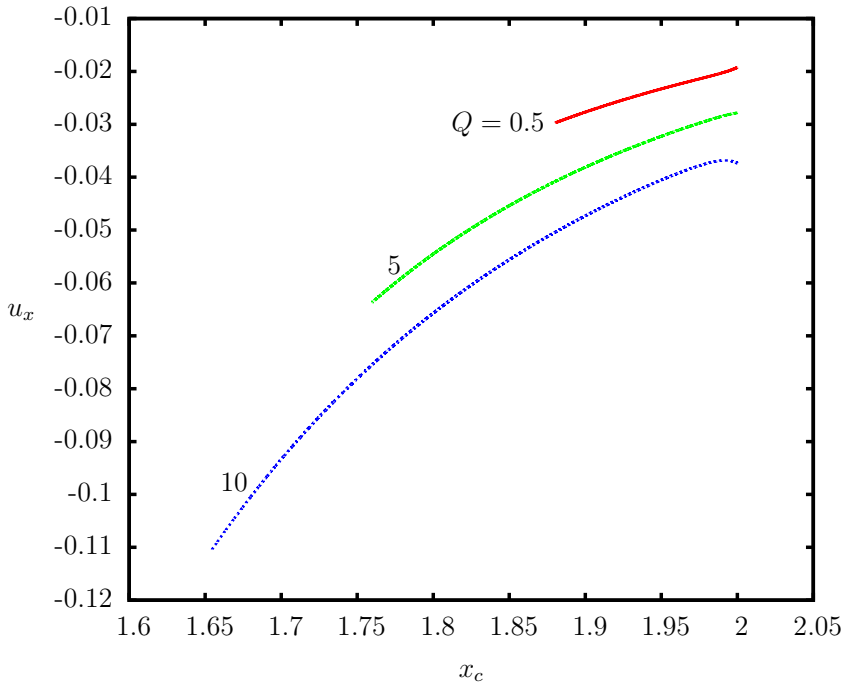

Figure 19. Droplet centroid velocity u_x as a function of location x_c under the influence of Q. $Ca_E = 0.2$, $R = 0.5$, $L = 2$ and $\lambda = 1$.

5.1.2. Droplet deformation

Electric properties of fluids not only affect the migration of the droplet under the non-uniform electric field, but also have strong influence on the droplet deformation D. The permittivity ratio Q influences the droplet deformation significantly as shown in Fig. 20. From this figure, we could find that the droplet has a big deformation at the beginning, after that the deformation value slowly decreases as the droplet migrates. We also find the deformation increases with Q when the droplet moves to the weaker electric field. Fig. 21(a) and (b) show the droplet 2D shape in the xz plane. Fig. 21(c) and (d) show the 3D droplet geometry corresponding to the cases of (a) and (b). The two cases have the same parameters except for the Q value. As our previous discussion for $R > 1$, the profiles show the droplets move to the positive x direction with time increasing. Comparing the two cases, we could find that the droplet with a larger Q value elongates a little bit more in z direction and has a greater dimple on the interface.

The resistivity ratio R also influences the droplet deformation significantly. Fig. 22

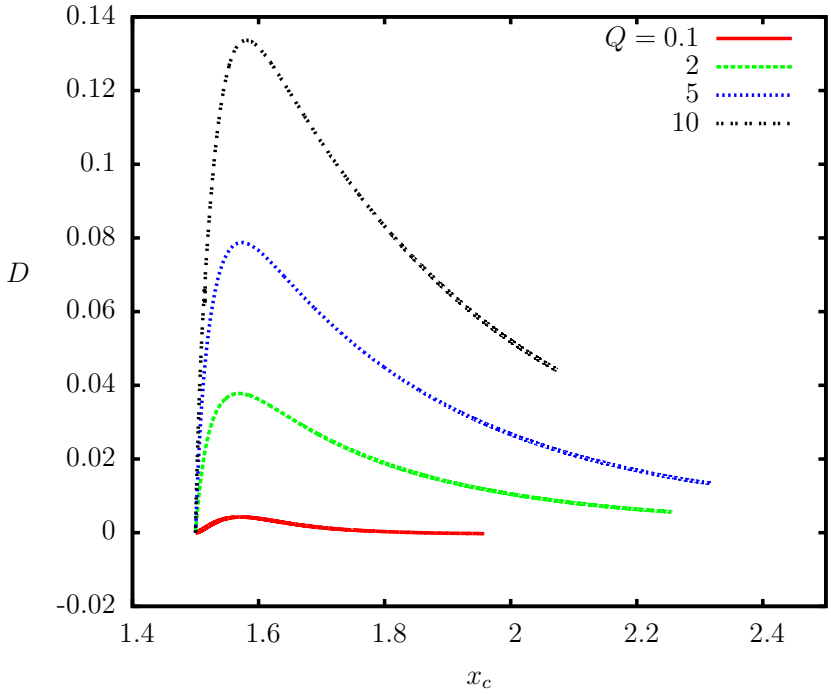

Figure 20. Droplet deformation D as a function of location x_c under the influence of Q. $R = 2$, $Ca_E = 0.2$, $L = 1.5$ and $\lambda = 1$.

shows the influence of R on the droplet deformation for the case of droplet migration to the weaker electric field. The droplet deformation increases as R increases when the droplet moves to the direction away from the point charge. When R is larger than 30, the influence of R on the deformation is negligibly small. Comparing Fig. 23 with Fig. 21 (a) and (c), we could find that a greater dimple is developed for a larger R.

When the droplet moves to the stronger electric field, the droplet deformation has demonstrated a more complicated behavior which is influenced by the permittivity ratio Q and the resistivity ratio R. For example in Fig. 24, the deformation D is positive for larger Q while the negative deformation value is observed with a smaller Q. The similar situation could be found for the influence of R on the droplet deformation. As shown in Fig. 25, when $R = 0.5$ the D is positive; when $R = 0.4$, the deformation value may exhibit positive first, and then turn negative; the droplet shows negative deformation throughout the entire process when $R \leq 0.3$.

The droplet may deform into two different kinds of shapes when it migrates towards

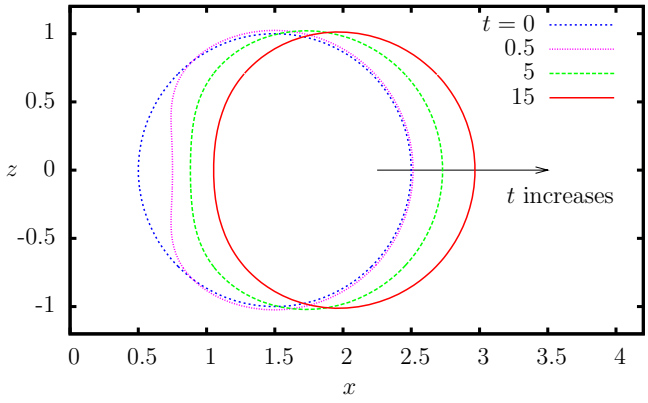

(a)

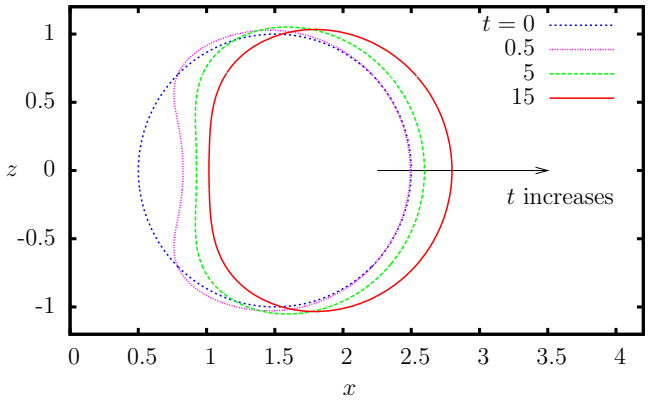

(b)

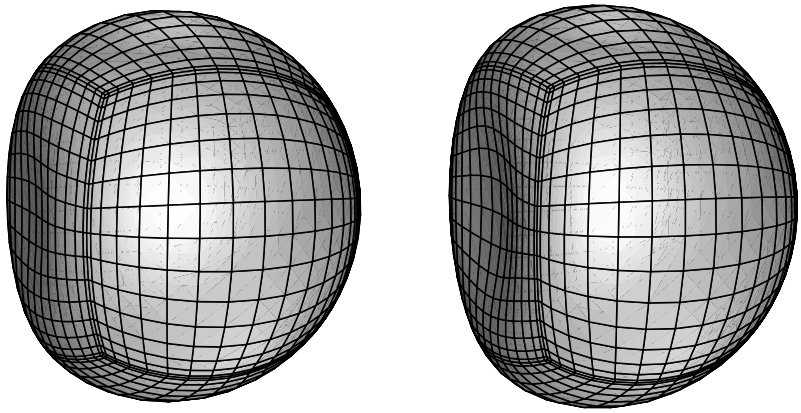

(c) (d)

Figure 21. Droplet shapes at different time t for $L = 1.5$ and $\lambda = 1$: (a) profiles for $R = 2$, $Q = 5$, $Ca_E = 0.2$, (b) profiles for $R = 2$, $Q = 10$, $Ca_E = 0.2$, (c) the 3D shape for case (a) at time $t = 0.5$, and (d) the 3D shape for case (b) at time $t = 0.5$.

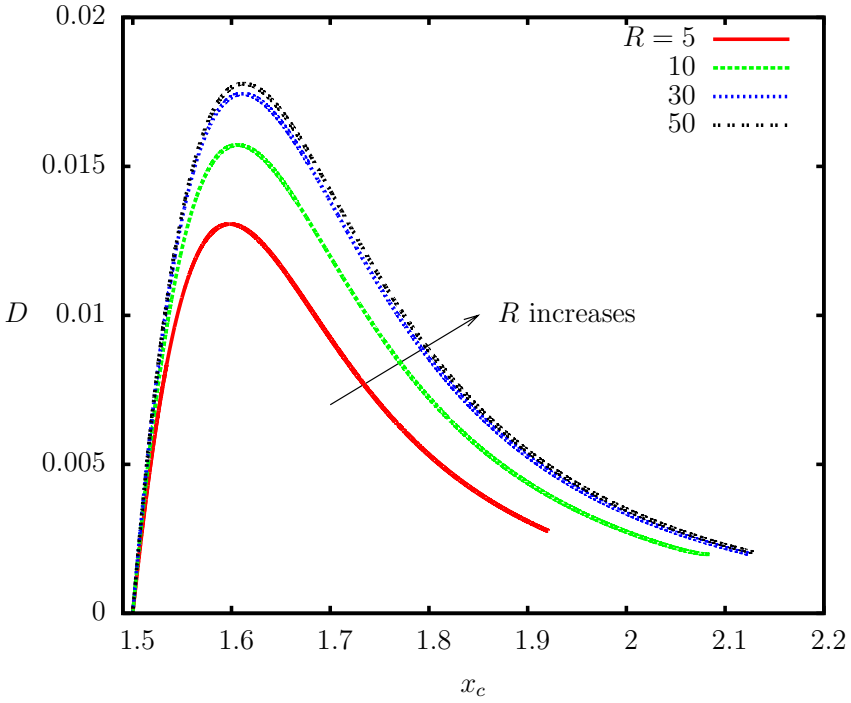

Figure 22. Droplet deformation D as a function of location x_c under the influence of R. $Q = 0.1$, $Ca_E = 0.2$, $L = 1.5$ and $\lambda = 1$.

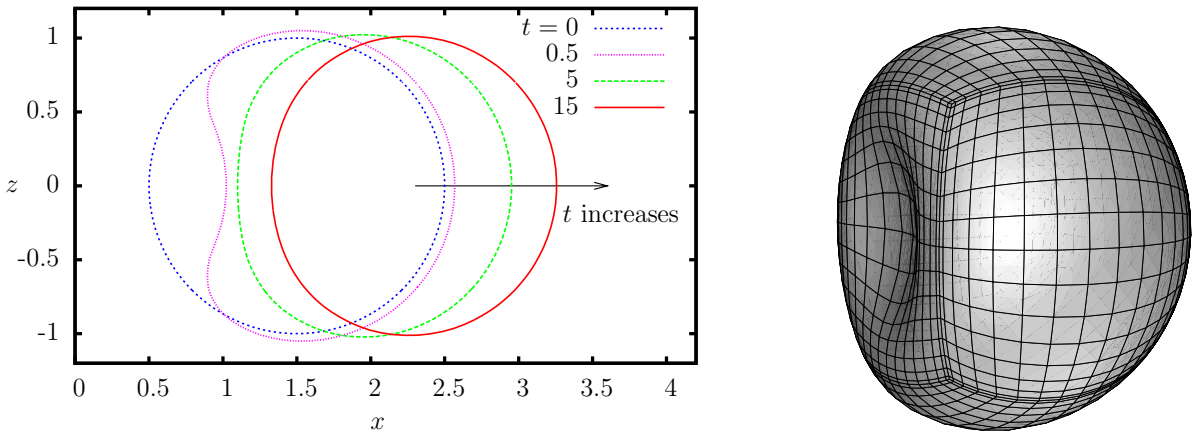

(a) (b)

Figure 23. Droplet shapes for $R = 30$, $Q = 5$, $Ca_E = 0.2$, $L = 1.5$ and $\lambda = 1$: (a) droplet profiles at different time t, and (b) the three-dimensional geometry of the droplet at time $t = 0.5$.

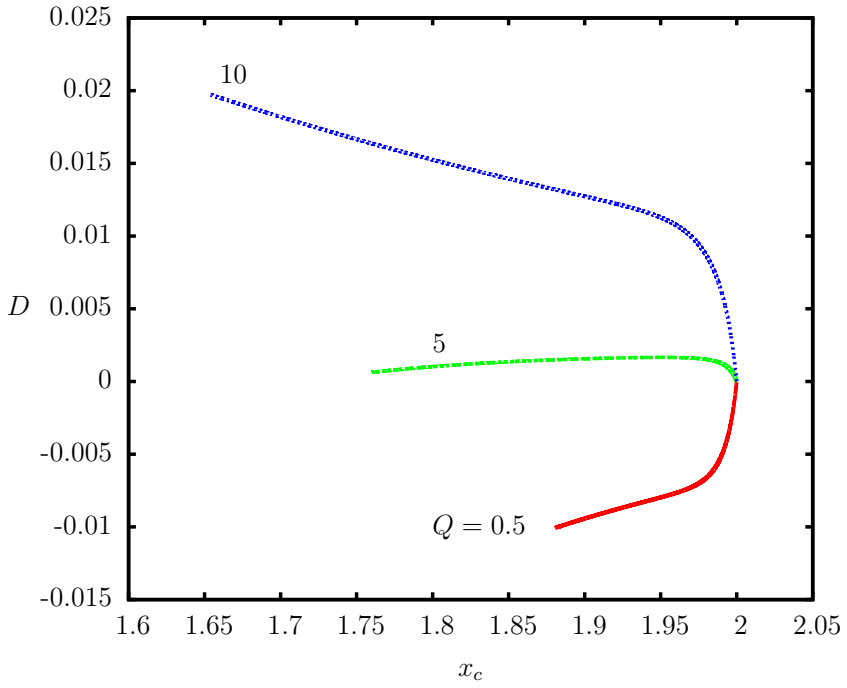

Figure 24. Droplet deformation D as a function of droplet centroid location x_c under the influence of Q. $Ca_E = 0.2$, $R = 0.5$, $L = 2$ and $\lambda = 1$.

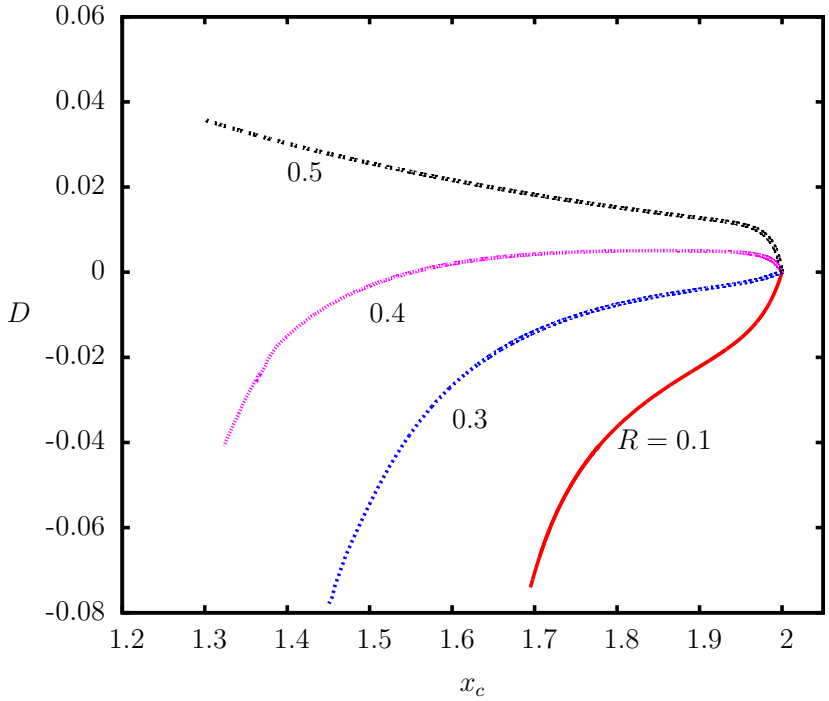

Figure 25. Droplet deformation D as a function of location x_c under the influence of R. $Ca_E = 0.2$, $Q = 10$, $R < 1$, $L = 2$ and $\lambda = 1$.

the point charge according to different R and Q values. The transient behavior of the droplet in the xz plane was shown in Fig. 26. A sharp tip on the interface of the droplet at the region closer to the point charge is generated when the droplet moves to the point charge in Fig. 26 (a) and (c). A 3D image of this shape is shown in Fig. 27. Another deformed shape is shown in Fig. 26 (b), where a dimple is developed in the area close to the point charge when the droplet moves close enough to the point charge.

Fig. 28 reveals the comprehensive behavior of the droplet deformation influenced by R and Q values. This diagram is not influenced by the electric capillary number Ca_E or the viscosity ratio λ. In this figure, the droplet deformation D is negative for the area below the curve. For the area above and in the vicinity of the curve, the deformation will have a positive value first and soon become negative as the droplet moves to the stronger electric field (the curve for $R = 0.4$ in Fig. 25 can be an example). The droplet deformation remains positive throughout the process for the area far above the curve.

Fig. 29 shows the time to that the droplet needs to get the maximum deformation under the influence of R and Q. From this figure, we find that t_D decreases with increasing Q, but it increases with increasing R. When R is larger than 10, the influence of R is negligible.

5.2. Influence of the electric capillary number

Ca_E exhibits significant influence on the droplet behavior. Fig. 30 shows the droplet deformation D as a function of the distance between the droplet centroid and the point charge x_c under the influence of Ca_E when the droplet moves to the weaker electric field. Fig. 31 shows the case of the droplet moving to the stronger electric field. Though Fig. 32 also shows the droplet moving to the point charge, the droplet deformation is positive. From those figures, we find that the droplet deformation monotony increases with Ca_E no matter what direction of the droplet migrates to or if the deformation value is positive or negative.

We also plot the droplet centroid velocity u_x as a function of the droplet location x_c for different values of Ca_E when the droplet migrates away from the point charge as shown in Fig. 33 and when the droplet migrates to the point charge as shown in Fig. 34. The

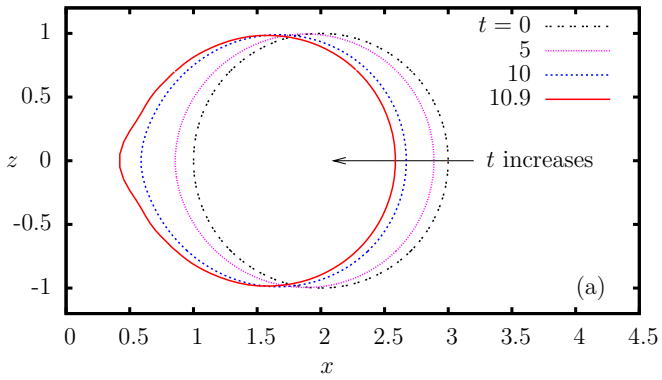

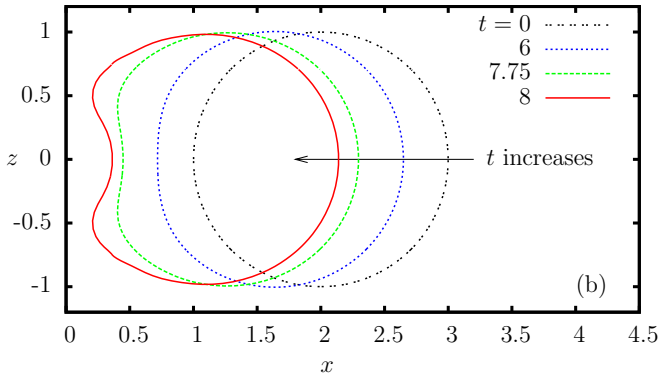

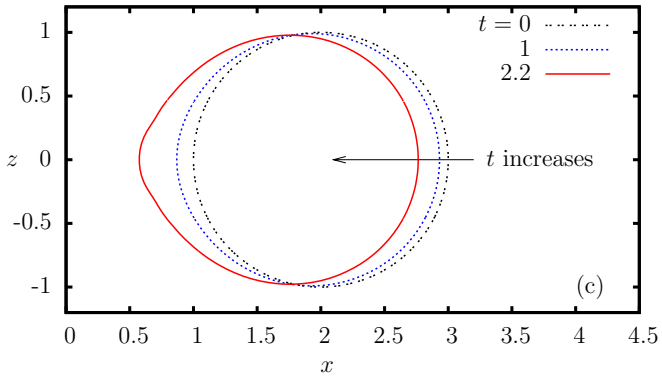

Figure 26. Profiles of a droplet with $Ca_E = 0.2$, $L = 1.5$ and $\lambda = 1$ at different time t. (a) $R = 0.5$, $Q = 0.5$. (b) $R = 0.5$, $Q = 10$. (c) $R = 0.1$, $Q = 10$.

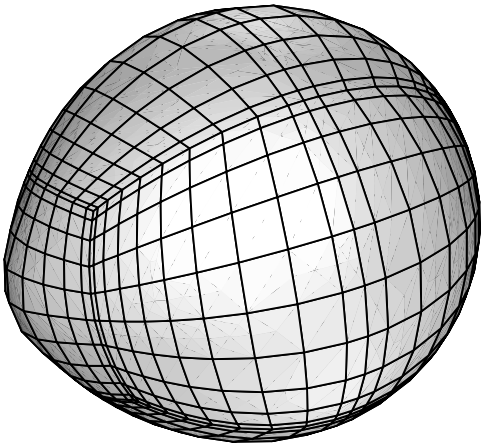

Figure 27. The three-dimensional geometry of a droplet at time $t = 2.2$ with $Q = 10$, $R = 0.1$, $\lambda = 1$, $Ca_E = 0.2$ and $L = 1.5$.

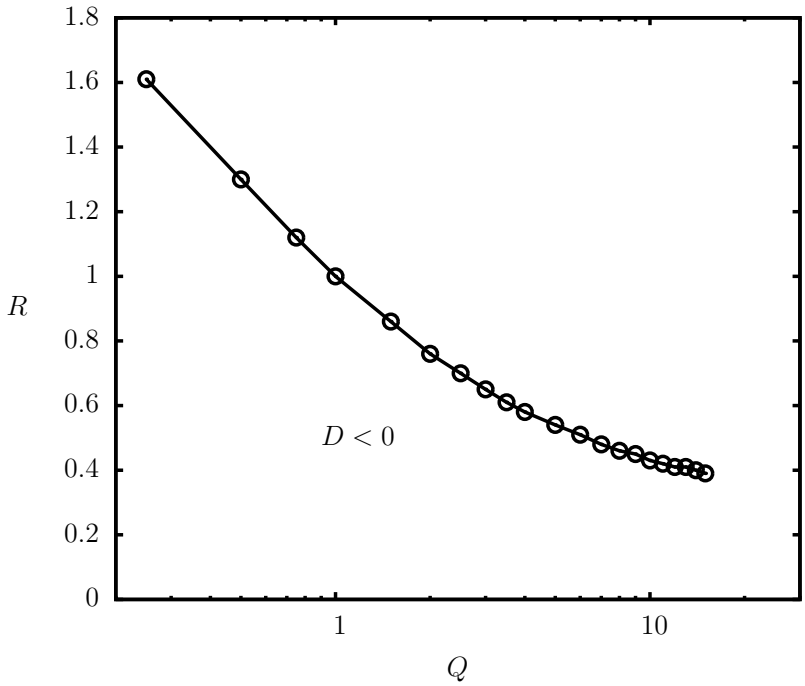

Figure 28. The Q-R diagram for the deformation D of a droplet initially located at a distance $L = 1.5$ towards the point charge which creates a non-uniform electric field.

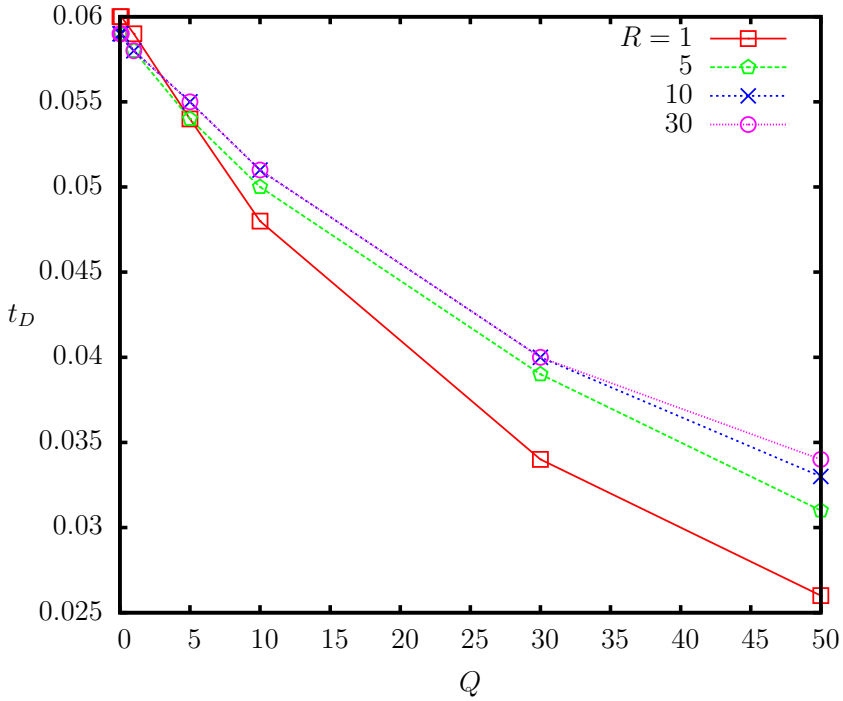

Figure 29. The time to that the droplet used to reach the maximum deformation as the function of Q and R when $Ca_E = 0.2$, $L = 2$ and $\lambda = 1$.

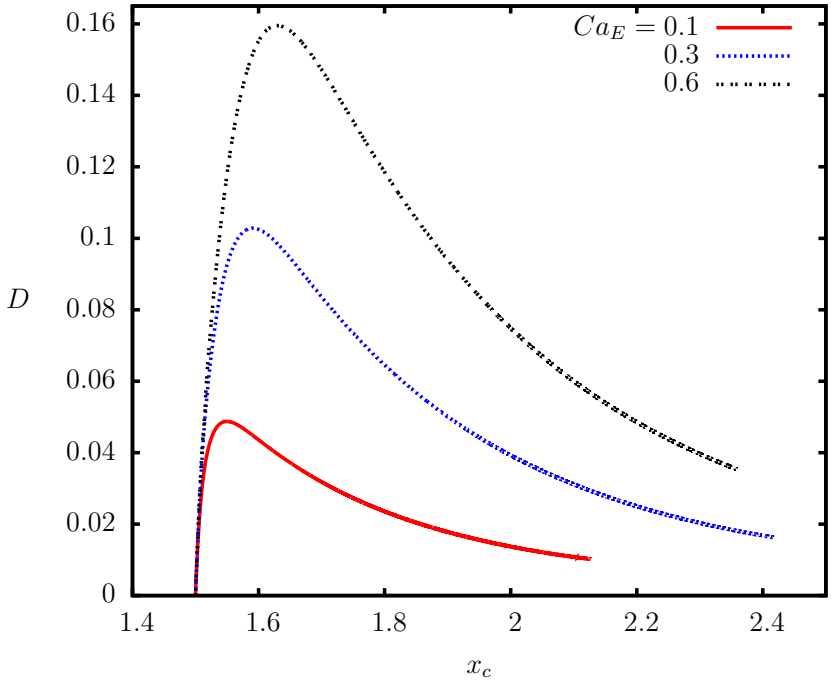

Figure 30. Droplet deformation D as a function of location x_c under the influence of Ca_E. $R = 2$, $Q = 5$, $L = 1.5$ and $\lambda = 1$.

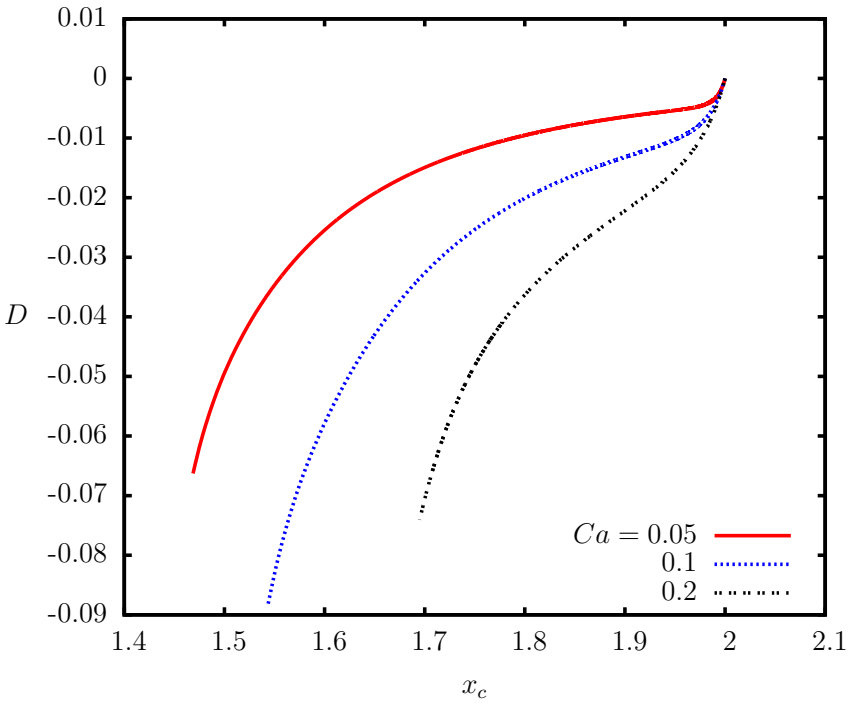

Figure 31. Droplet deformation D as a function of location x_c under the influence of Ca_E. $Q = 10$, $R = 0.1$, $L = 2$ and $\lambda = 1$.

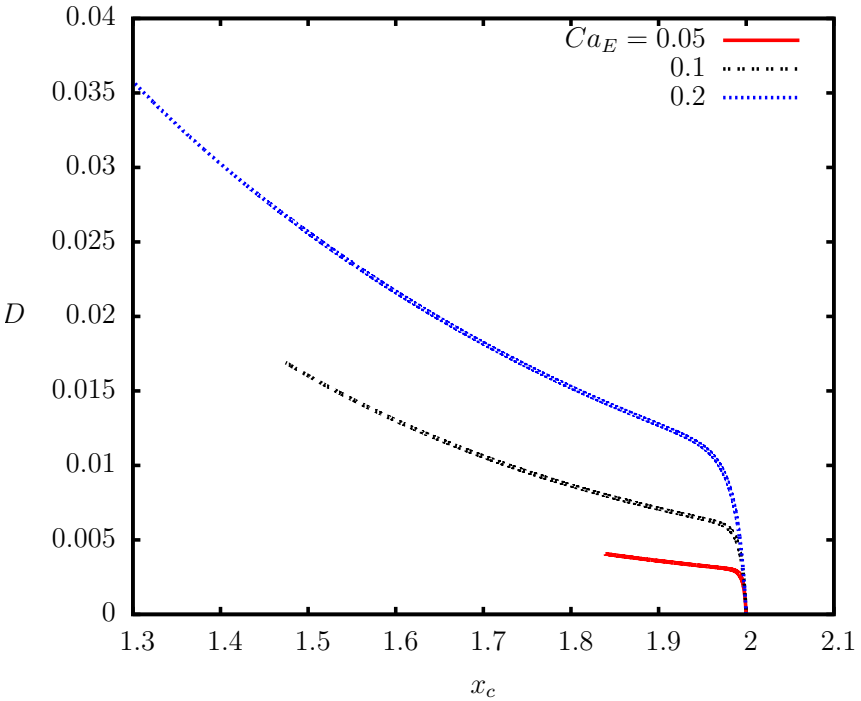

Figure 32. Droplet deformation D as a function of location x_c under the influence of Ca_E. $Q = 10$, $R = 0.5$, $L = 2$ and $\lambda = 1$.

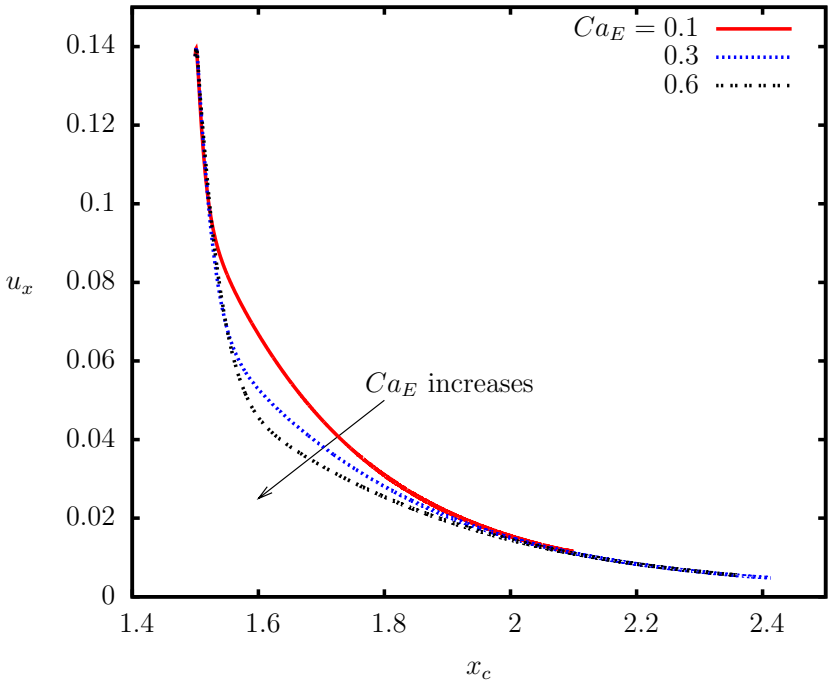

Figure 33. Droplet centroid velocity u_x as a function of location x_c under the influence of Ca_E. $R = 2$, $Q = 5$, $L = 1.5$ and $\lambda = 1$.

figures show that the droplet migration direction is not affected by Ca_E, instead, a larger Ca_E value could lead to more abrupt changes in migration velocity. In Fig. 33, the droplet with different Ca_E have the same velocity when they are released at the beginning. The droplet then experiences a more abrupt decrease in its migration velocity with a larger Ca_E. At the end the droplets have the same velocity under different Ca_E. In Fig. 34, for droplets migrating towards the point charge, the velocity for droplets with different Ca_E start to become distinctive when x_c is close to 1.8. After that, the velocity difference increases as the droplet migrates. Fig. 35 shows the time for the droplet to reach the maximum deformation increases as Ca_E increases.

5.3. Influence of the viscosity ratio

A larger viscosity ratio means the droplet fluid is much more viscous than the surrounded liquid. We find the droplet with a larger viscosity ratio generally has a slower migration speed and a smaller deformation value than the droplet with a smaller viscosity ratio based on computational results. We plot Fig. 36 for a droplet moves to the weaker

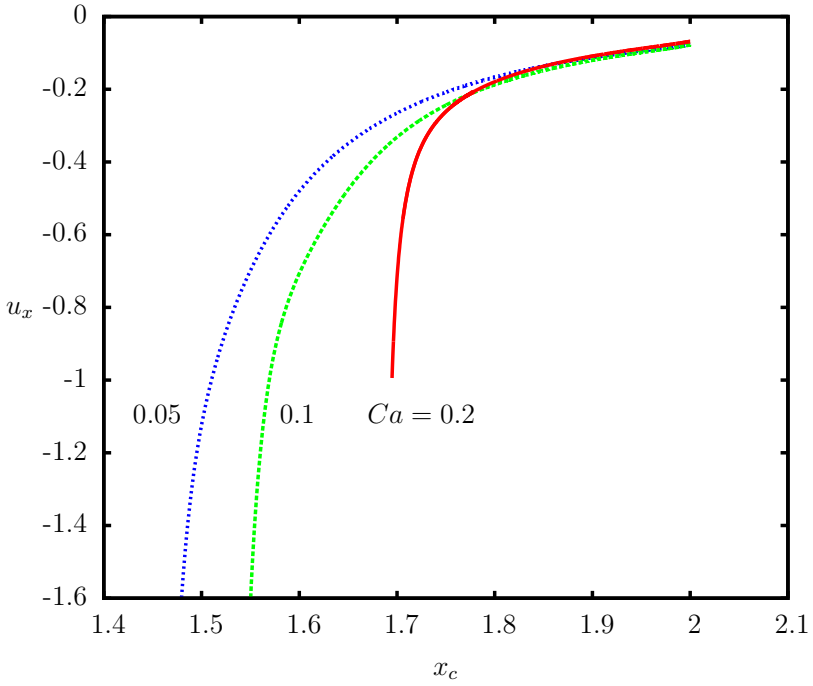

Figure 34. Droplet centroid velocity u_x as a function of location x_c under the influence Ca_E. $Q = 10$, $R = 0.1$, $L = 2$ and $\lambda = 1$.

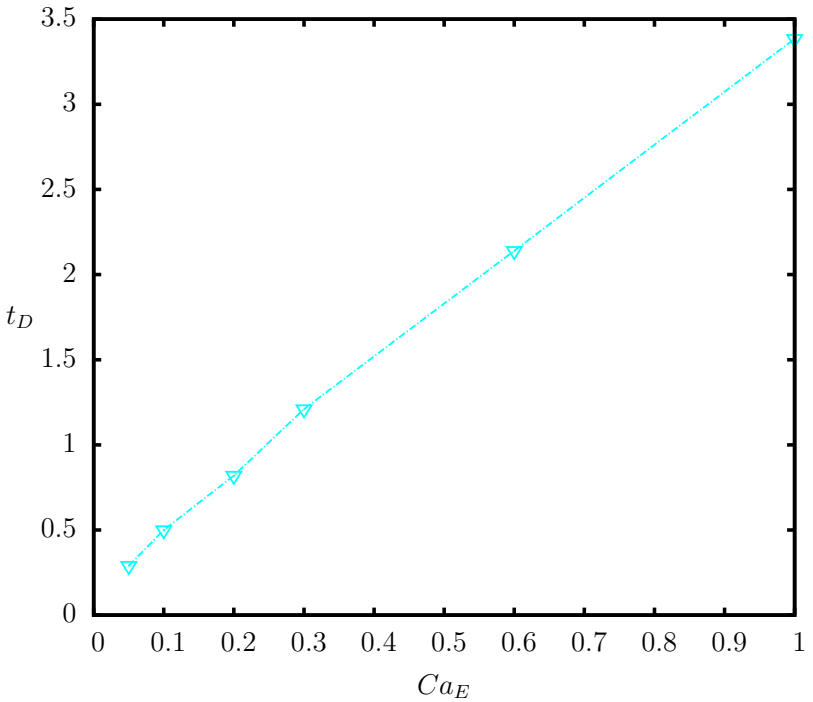

Figure 35. The time that the droplet needs to reach the maximum deformation as the function of Ca_E. $R = 2$, $Q = 5$, $\lambda = 1$ and $L = 1.5$.

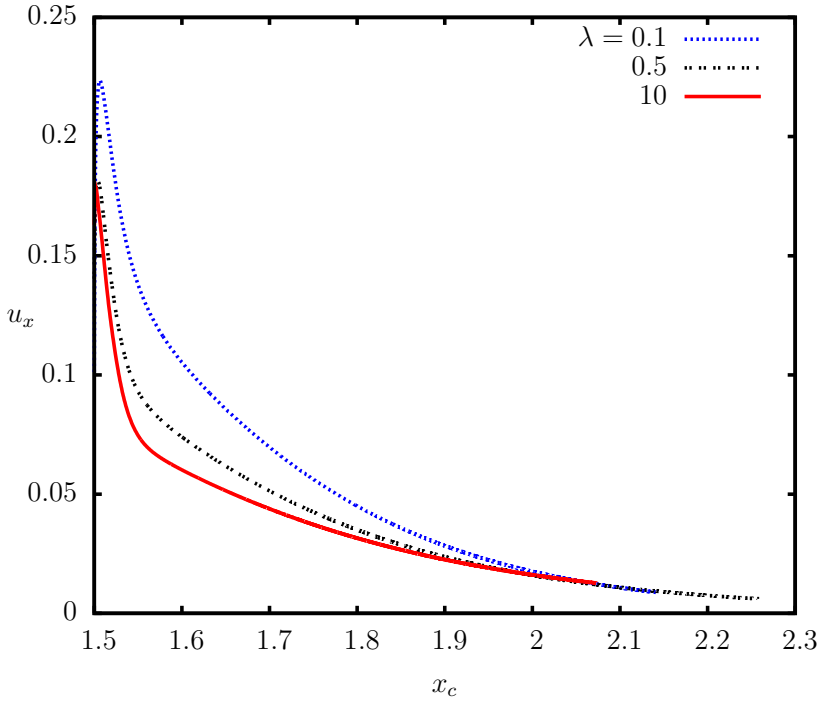

Figure 36. Droplet velocity u_x as a function of location x_c under the influence of λ. For all cases, $Q = 10$, $R = 2$, $Ca_E = 0.2$ and $L = 1.5$.

electric field and Fig. 37 for a droplet migrating towards a stronger electric field. No matter what direction the droplet moves, larger viscosity ratio reduces the droplet speed. Especially when the droplet moves to the point charge, the viscosity ratio λ has a significant influence on the droplet velocity. A larger λ not only tends to decrease the droplet viscosity, but also has a big effect on the droplet deformation when the droplet moves to the direction of the point charge, such as Fig. 38. It is because a larger value in λ corresponding to a more viscous droplet leads to the slower response to the electric force. But when the droplet moves to the weaker electric field, this influence is small for different λ as shown in Fig. 39. Fig. 40 reveals that the time for the droplet to reach the maximum deformation is increasing with λ increasing when $\lambda < 10$. A plateau is found when $\lambda > 10$.

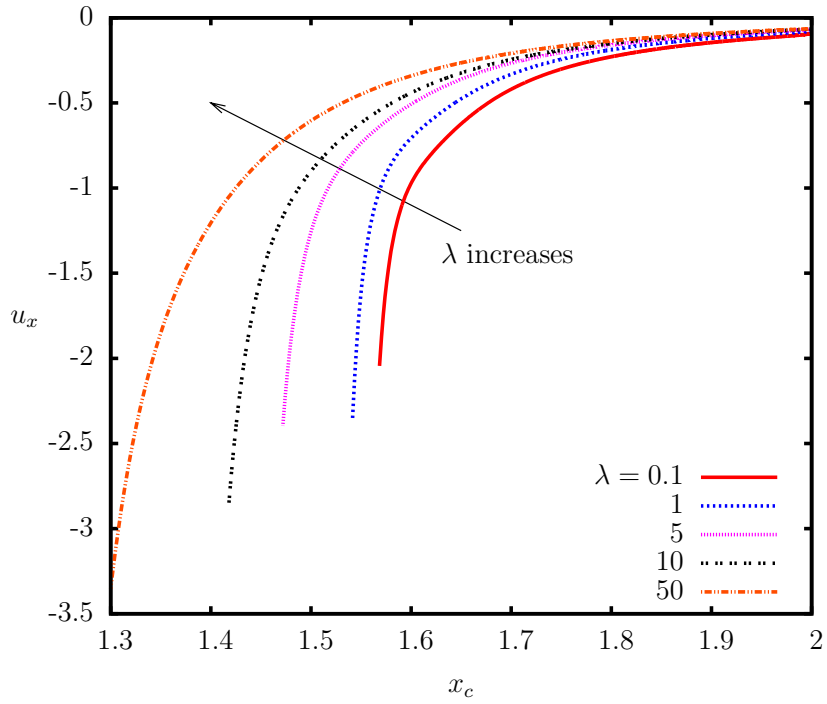

Figure 37. Droplet velocity u_x as a function of location x_c under the influence of λ. For all cases, $Q = 10$, $R = 0.1$, $Ca_E = 0.1$ and $L = 2$.

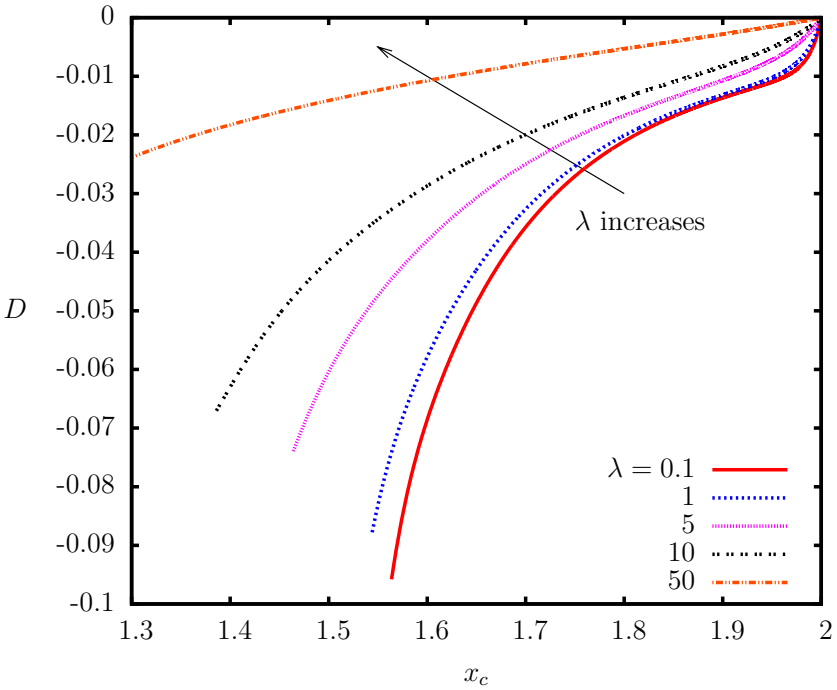

Figure 38. Droplet deformation D as a function of location x_c under the influence of λ. For all cases, $Q = 10$, $R = 0.1$, $Ca_E = 0.1$ and $L = 2$.

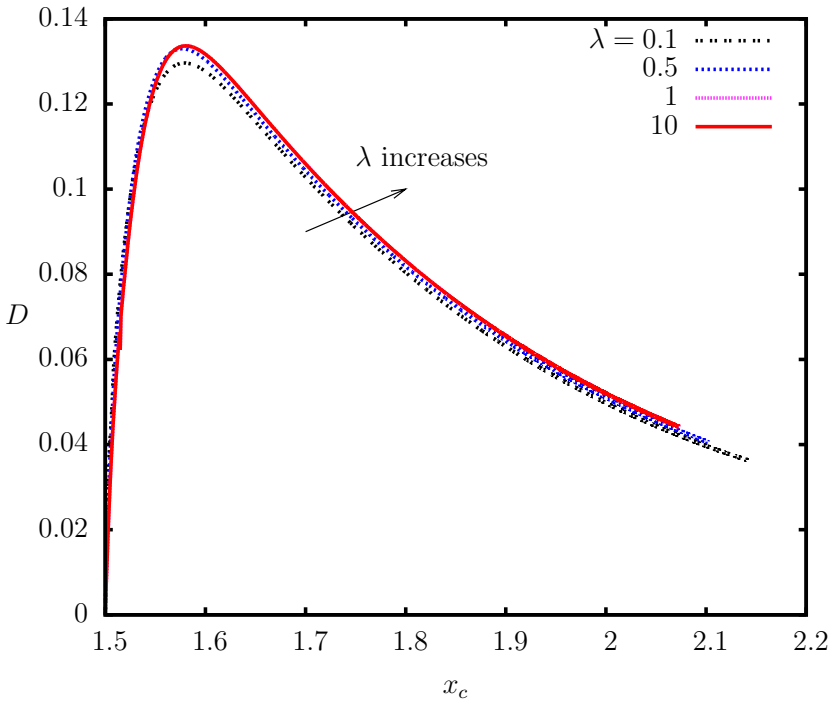

Figure 39. Droplet deformation D as a function of location x_c under the influence of λ. For all cases, $Q = 10$, $R = 2$, $Ca_E = 0.2$ and $L = 1.5$.

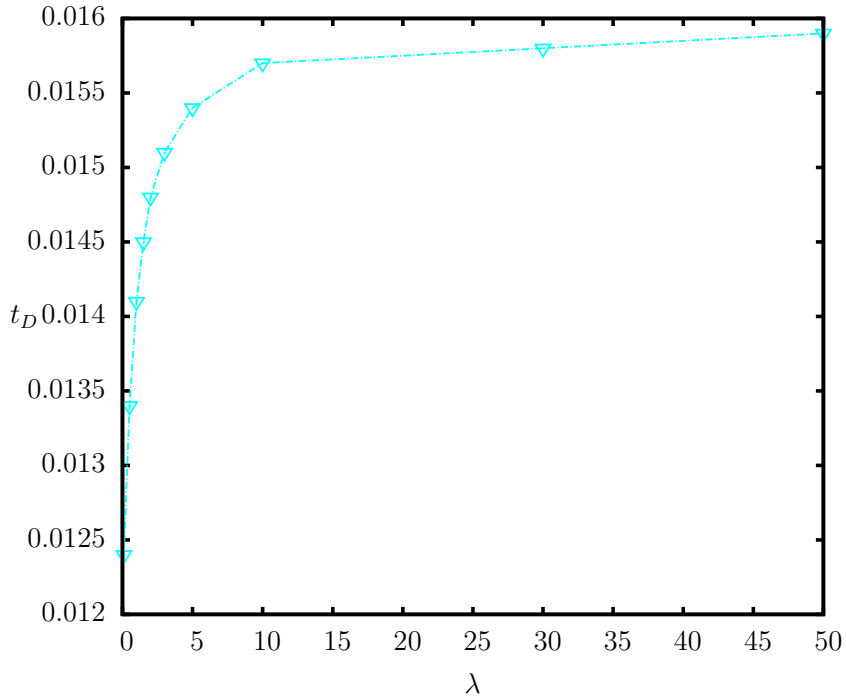

Figure 40. The time that the droplet needs to reach the maximum deformation as the function of λ. $R = 2$, $Q = 10$, $Ca_E = 0.2$ and $L = 1.5$.

CHAPTER 6. PERFECT DIELECTRIC DROPLET BEHAVIOR IN A NON-UNIFORM ELECTRIC FIELD

For a perfect dielectric system, conductivity is not considered for the droplet and the surrounding liquid, so the resistivity ratio R does not exist in our computation. In this part, we introduce how permittivity ratio Q, capillary number Ca_E and viscosity ratio μ influence the droplet movement and deformation for the perfect dielectric system affected by a non-uniform electric field. Comparisons of the leaky dielectric droplet system and the perfect dielectric droplet system are carried out. In comparison, parameters Ca_E, L and λ are identical for the two systems. For the leaky dielectric system, the resistivity ratio is maintained as $R = 1$ in our computations throughout this section.

6.1. Influence of electric properties of fluids

When the droplet permittivity is larger than the surrounding liquid permittivity ($Q > 1$), the droplet moves to the stronger electric field no matter it is a leaky dielectric system or a perfect dielectric system. On the contrary, when $Q < 1$, the droplet permittivity is less than the surrounding liquid permittivity, the droplet moves to the weaker electric field. Just like Fig. 41 when $Q < 1$ x_c increases with time, which means the droplet migrates to the weaker electric field; when $Q > 1$, x_c decreases as the time increases, which means the droplet moves in the direction of the point charge, in the other words, the droplet moves to the stronger electric field; and when $Q = 1$ the droplet stays at the original position. Fig. 41 (a) is for a perfect dielectric system and Fig. 41 (b) is for a leaky dielectric system.

By examining the travel distance of the droplet in Fig. 41 (a) and Fig. 41 (b), we find that the droplet in the perfect dielectric system moves faster than the droplet in the leaky dielectric system with the same time consuming. Fig. 42 (a) and (b) show droplet centroid velocity u_x as a function of location x_c for a perfect dielectric system and a leaky dielectric system respectively when $Q < 1$. For both systems the droplet velocity u_x decreases with Q increasing when $Q < 1$. The droplets for leaky dielectric system appear to have a much smaller migration velocity than those for a perfect dielectric system. Fig. 43 (a) and (b)

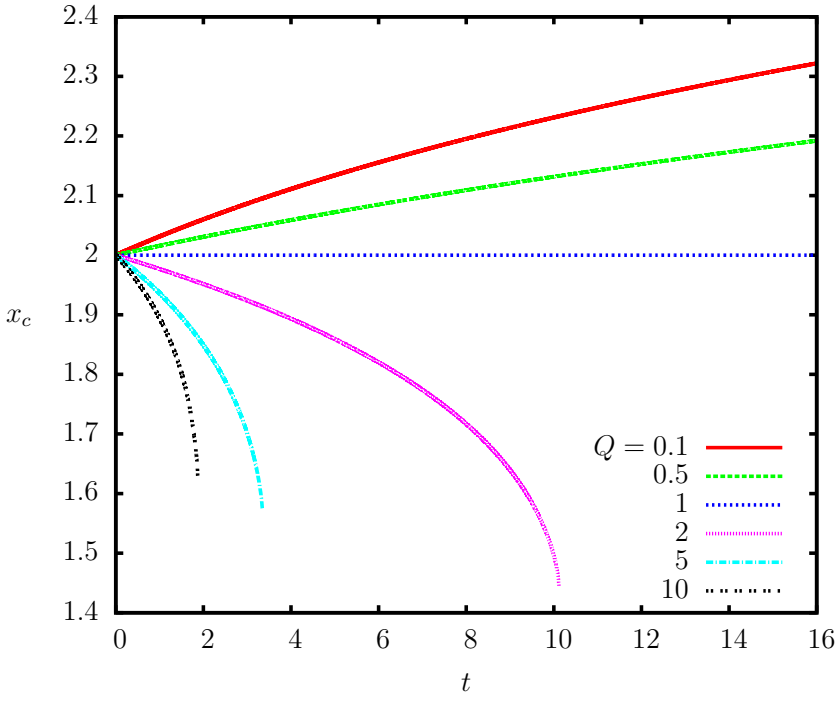

(a)

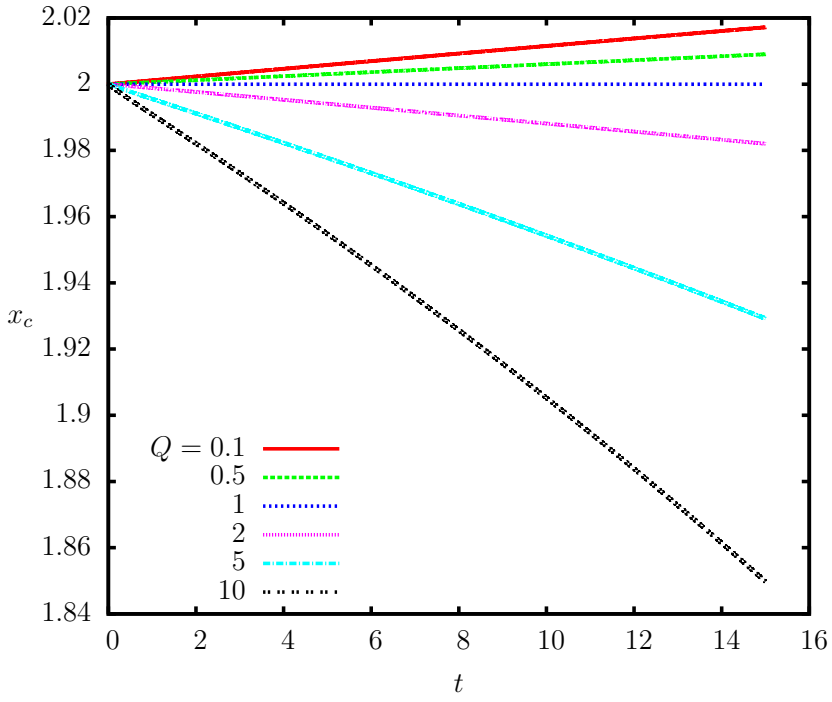

(b)

Figure 41. Droplet centroid location x_c as a function of time t under the influence of Q when $Ca_E = 0.2$, $L = 2$ and $\lambda = 1$. (a) Perfect dielectric system. (b) Leaky dielectric system.

show the similar plots, but the droplet moves to the stronger electric field when $Q > 1$. When $Q > 1$ the droplet velocity u_x increases with Q increasing for both of the systems. Again, we observe that the droplets migrate more slowly for a leaky dielectric system.

Fig. 44 (a) shows that $D > 0$ when $Q < 1$ for a perfect dielectric system and Fig. 44 (b) shows that $D < 0$ when $Q < 1$ for a leaky dielectric system. For both systems, the deformation D magnitude decreases as Q increases. The droplet deformation experiences a rapid increase at the beginning and then decreases slowly when the droplet moves to the weaker electric field for a perfect dielectric system. For leaky dielectric system, the deformation magnitude increases rapidly to the maximum first, and then a plateau is found. On the contrary, when $Q > 1$, $D < 0$ was found for a perfect dielectric system and $D > 0$ for a leaky dielectric system, as shown in Fig. 45. For both systems, the droplet deformation magnitude increases as Q increases when $Q > 1$. For the perfect dielectric system, when the droplet moves to the stronger electric field the deformation magnitude increases graduately, and then increases dramatically. But for the leaky dielectric system, the droplet deforms dramatically at the beginning, after the deformation reaches maximum a plateau could be found.

6.2. Influence of the electric capillary number

For the perfect dielectric system, the electric capillary number Ca_E does not alter the droplet moving direction, but has a big influence on the migration velocity and deformation of the droplet. Fig. 46 and Fig. 47 show how Ca_E affects the u_x when the droplet migrates towards the point charge. A larger electric capillary number pushes the droplet to its the maximum velocity with less time. The leaky dielectric system has the similar results, such as Fig. 34. When the droplet moves away from the point charge, the electric capillary number Ca_E has very small influence on the droplet velocity u_x, as shown in Fig. 48.

We plot the droplet deformation D as a function of the droplet location x_c for different values of Ca_E in Fig. 49 and Fig. 50. As shown in Fig. 49, when the droplet moves to the point charge, a larger Ca_E makes the droplet to deform more abruptly and severely.

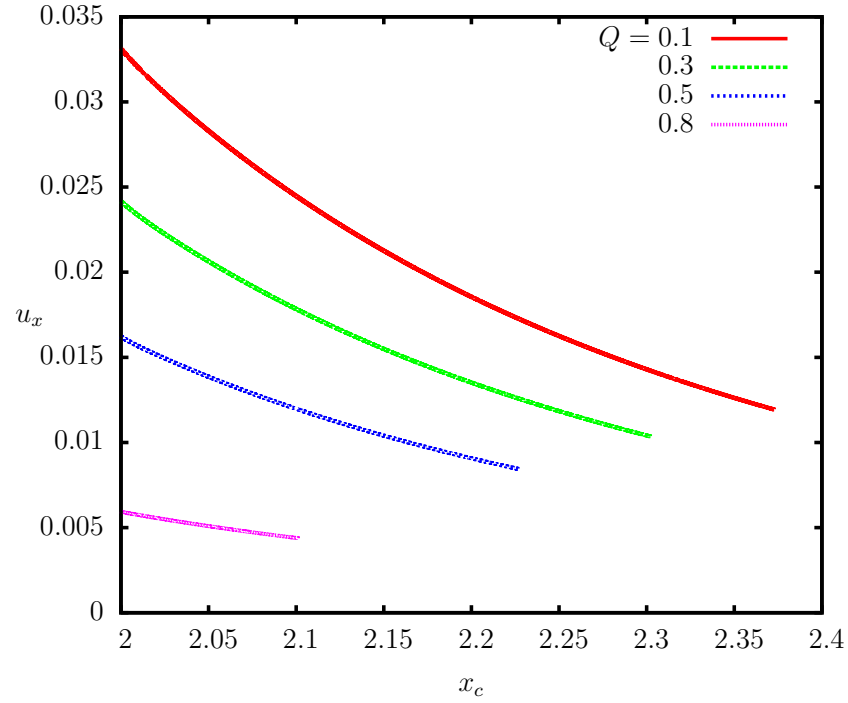

(a)

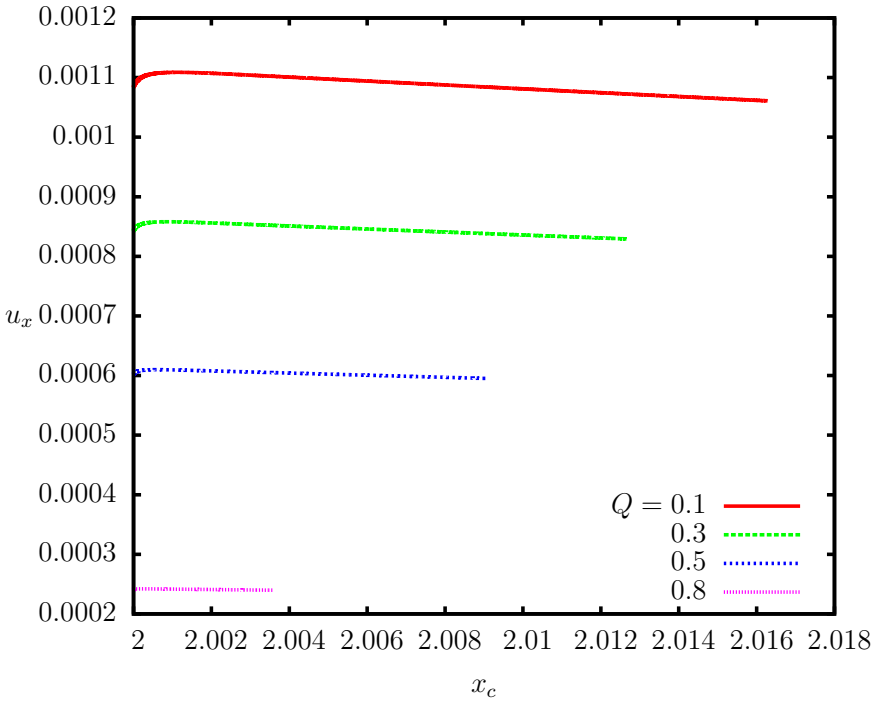

(b)

Figure 42. Droplet centroid velocity u_x as a function of location x_c under the influence of Q when $Q < 1$, $Ca_E = 0.2$, $L = 2$ and $\lambda = 1$. (a) Perfect dielectric system. (b) Leaky dielectric system.

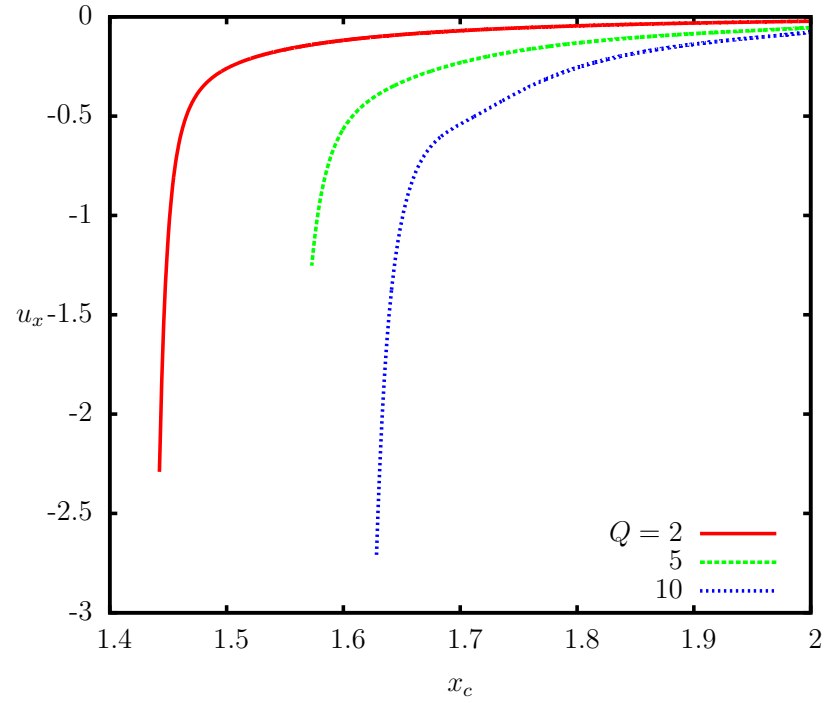

(a)

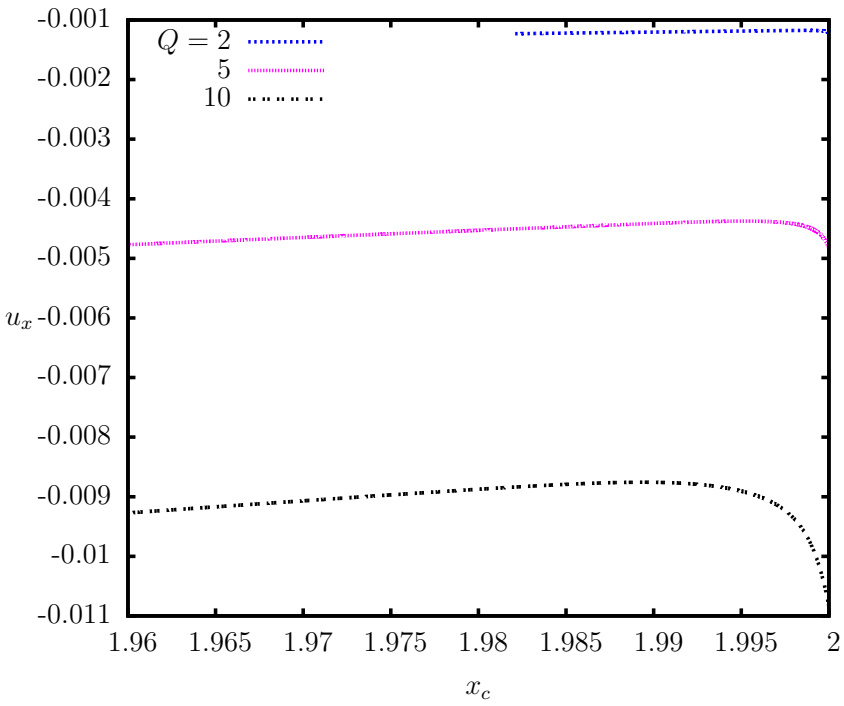

(b)

Figure 43. Droplet centroid velocity u_x as a function of location x_c under the influence of Q when $Q > 1$, $Ca_E = 0.2$, $L = 2$ and $\lambda = 1$. (a) Perfect dielectric system. (b) Leaky dielectric system.

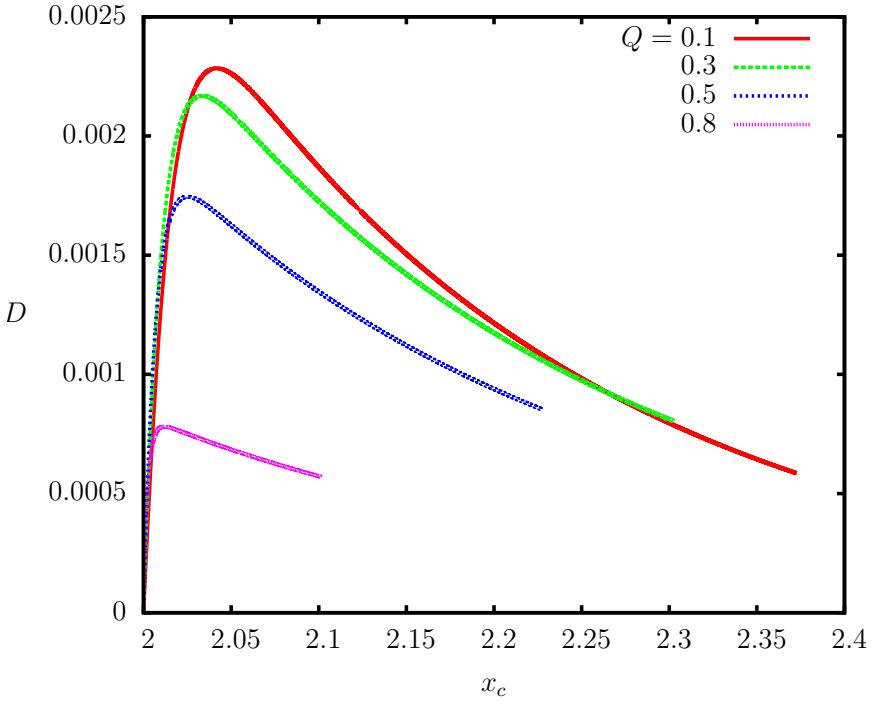

(a)

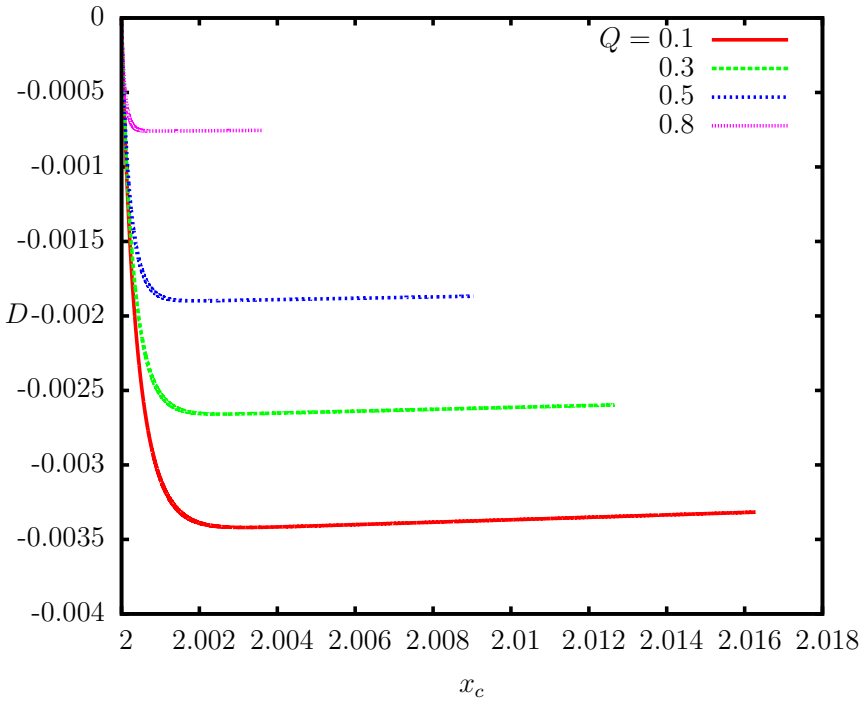

(b)

Figure 44. Droplet deformation D as a function of location x_c under the influence of Q when $Q < 1$, $Ca_E = 0.2$, $L = 2$ and $\lambda = 1$. (a) Perfect dielectric system. (b) Leaky dielectric system.

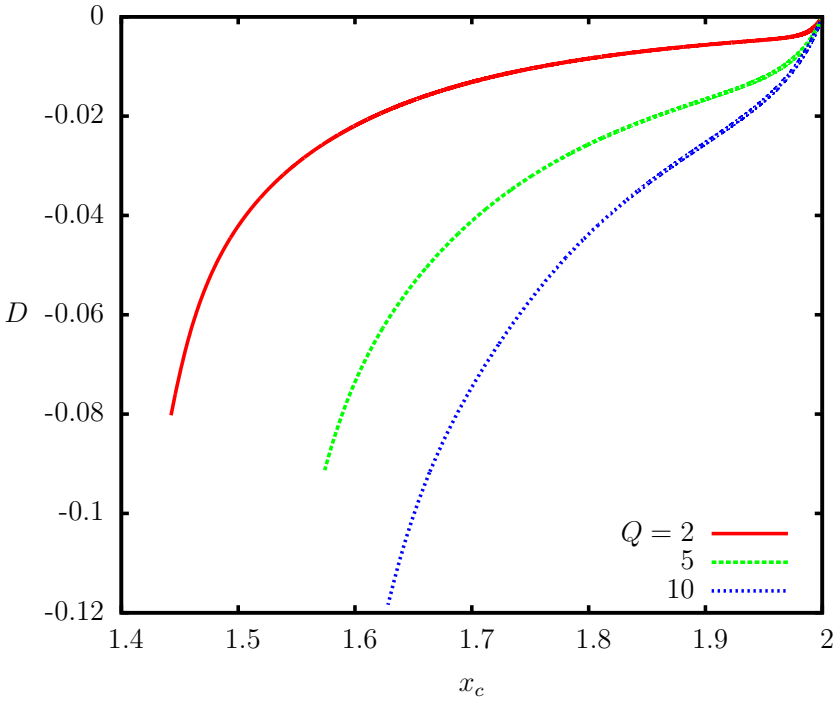

(a)

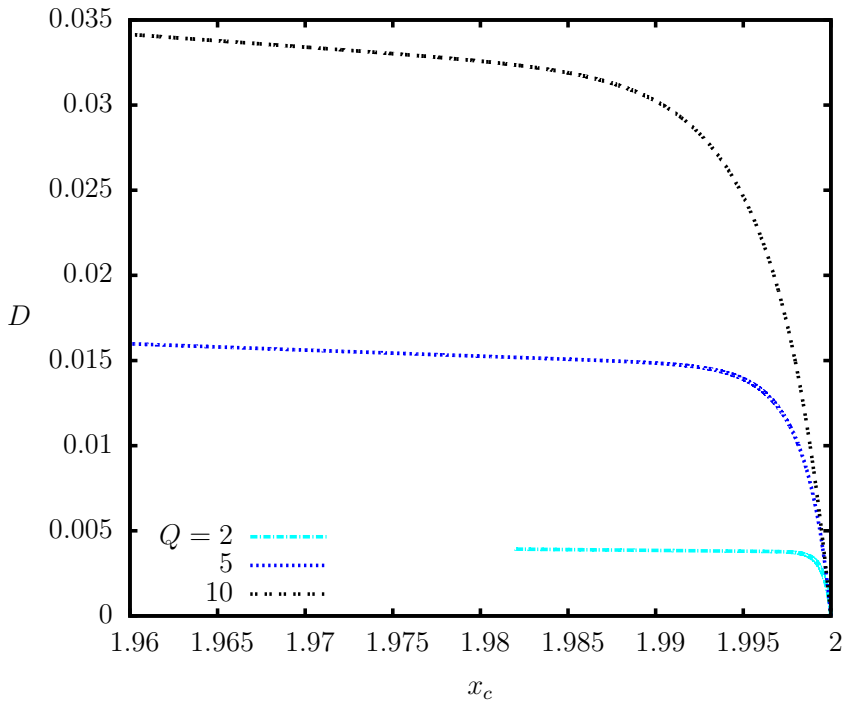

(b)

Figure 45. Droplet deformation D as a function of location x_c under the influence of Q when $Q > 1$, $Ca_E = 0.2$, $L = 2$ and $\lambda = 1$. (a) Perfect dielectric system. (b) Leaky dielectric system.

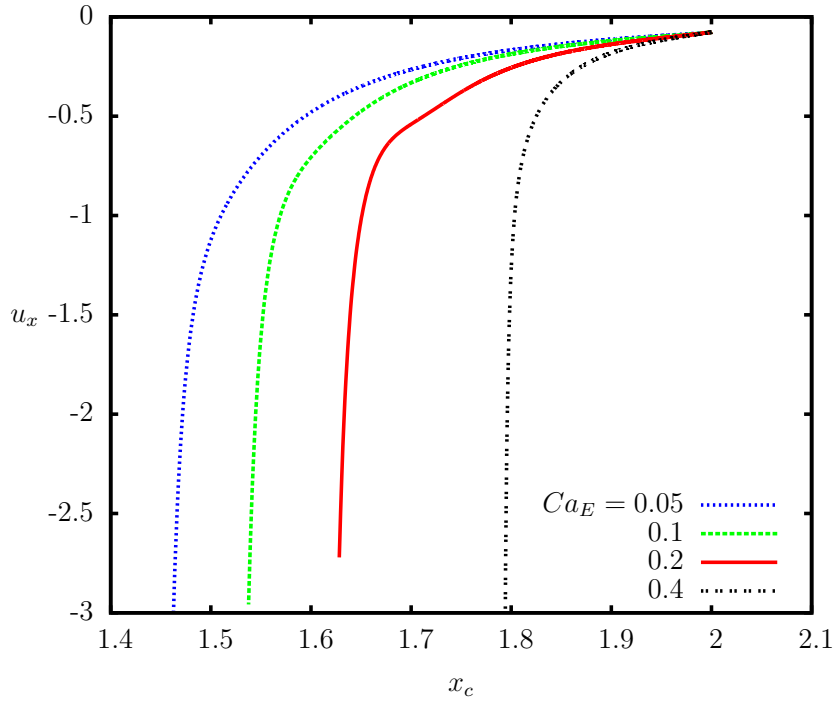

Figure 46. Droplet velocity u_x as a function of location x_c under the influence of Ca_E when $Q = 10$, $L = 2$ and $\lambda = 1$ for a perfect dielectric system.

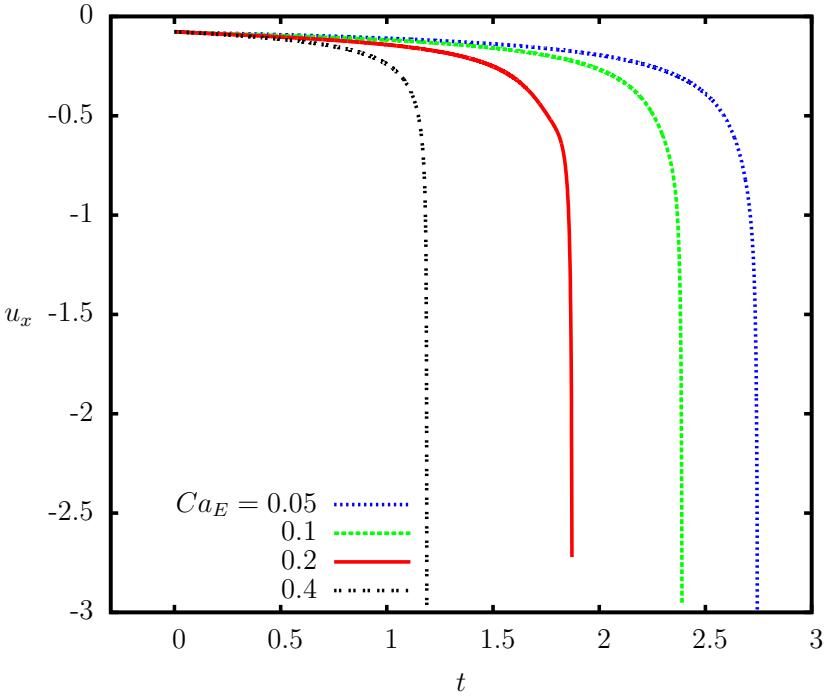

Figure 47. Droplet velocity u_x as a function of time t under the influence of Ca_E when $Q = 10$, $L = 2$ and $\lambda = 1$ for a perfect dielectric system.

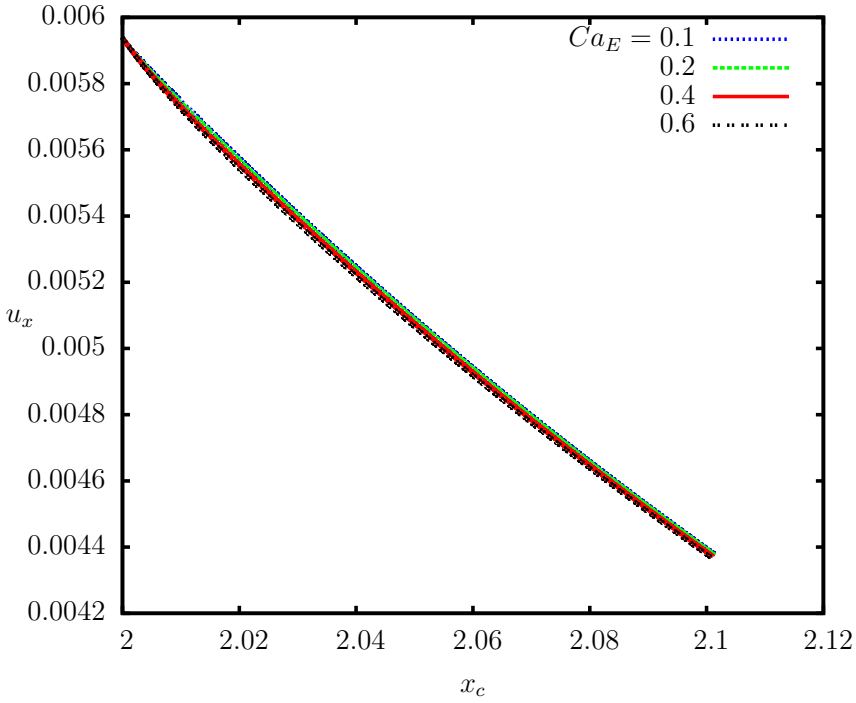

Figure 48. Droplet velocity u_x as a function of location x_c under the influence of Ca_E when $Q = 0.8$, $L = 2$ and $\lambda = 1$ for a perfect dielectric system.

When the droplet moves away from the point charge, the deformation reaches the maximum quickly at the beginning and then decreases slowly as the droplet moves further from the point charge. A larger deformation is achieved with a larger Ca_E in the perfect dielectric system.

6.3. Influence of the viscosity ratio

For a perfect dielectric system, a larger viscosity ratio λ usually tends to reduce the droplet velocity u_x without altering the droplet migration direction no matter what direction the droplet moves towards. Fig. 51 shows droplet migration velocity u_x as a function of x_c under the influence of λ. Unlike the leaky dielectric system shown in Fig. 36, λ has a big influence on droplet velocity throughout the entire droplet migration process. The droplet velocity keeps decreasing as the droplet moves away from the point charge. When the droplet moves towards the point charge as shown in Fig. 52, the increasing droplet speed shows a slower change in its magnitude for larger λ. This behavior is similar to that for a leaky dielectric system (Fig. 37).

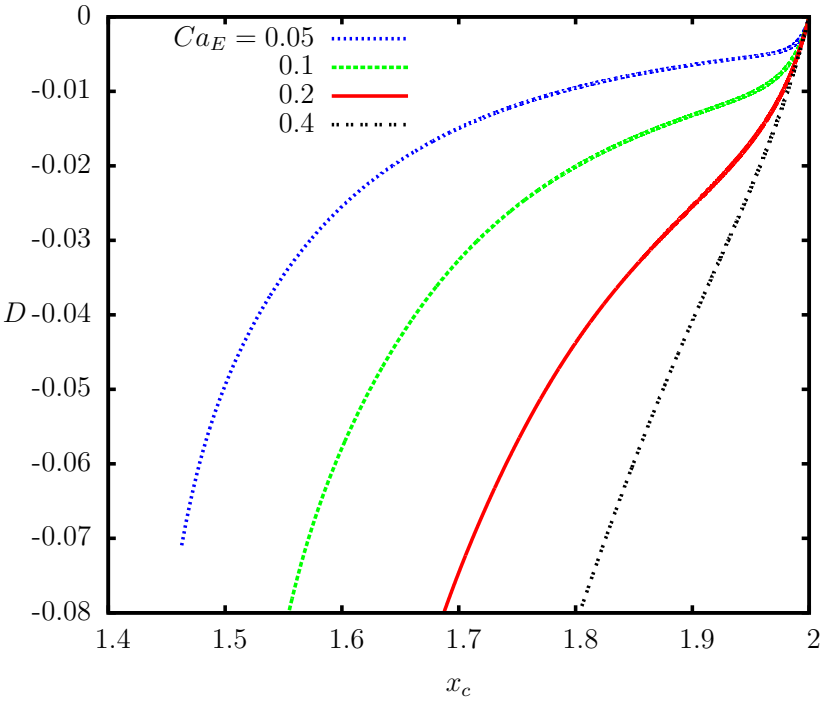

Figure 49. Droplet deformation D as a function of location x_c under the influence of Ca_E when $Q = 10$, $L = 2$ and $\lambda = 1$ for a perfect dielectric system.

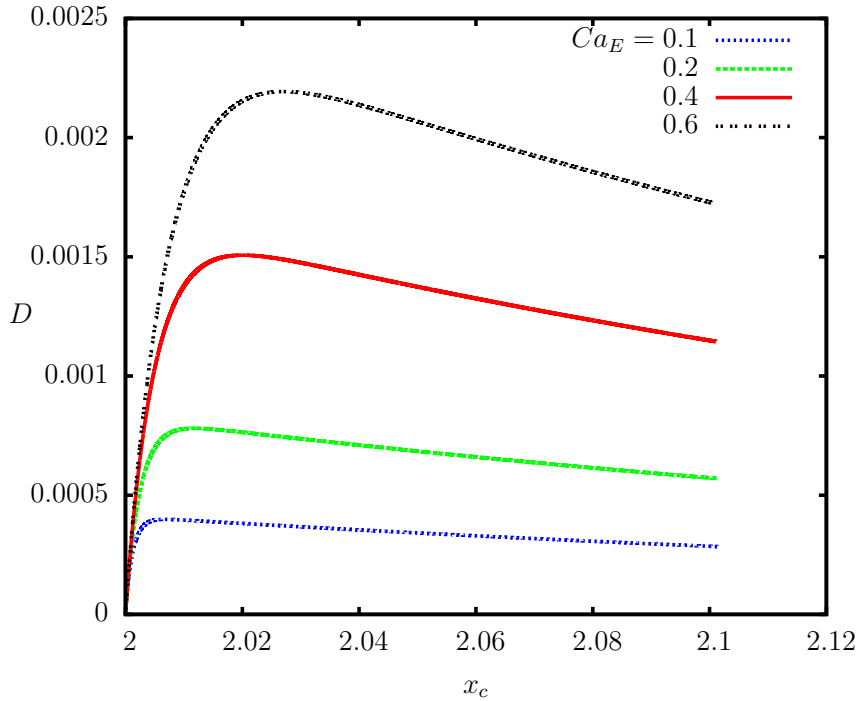

Figure 50. Droplet deformation D as a function of location x_c under the influence of Ca_E when $Q = 0.8$, $L = 2$ and $\lambda = 1$ for a perfect dielectric system.

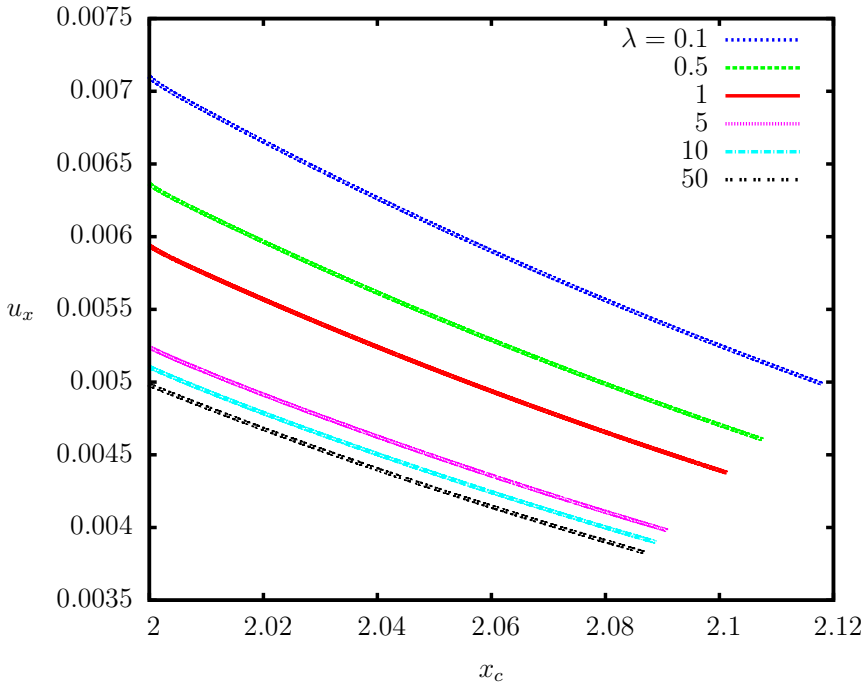

Figure 51. Droplet velocity u_x as a function of location x_c under the influence of λ when $Q = 0.8$, $L = 2$ and $Ca_E = 0.2$ for a perfect dielectric system.

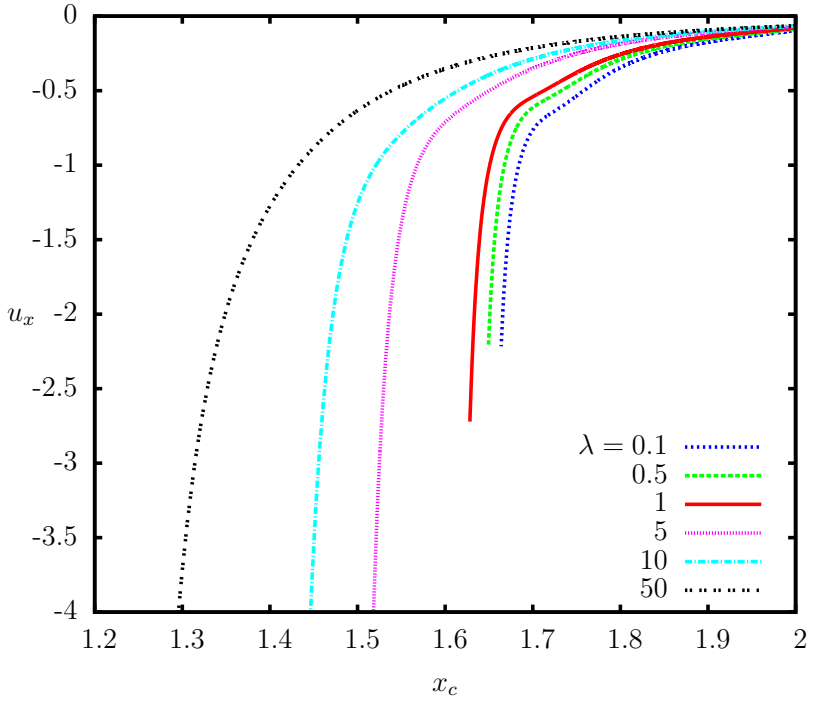

Figure 52. Droplet velocity u_x as a function of location x_c under the influence of λ when $Q = 10$, $L = 2$ and $Ca_E = 0.2$ for a perfect dielectric system.

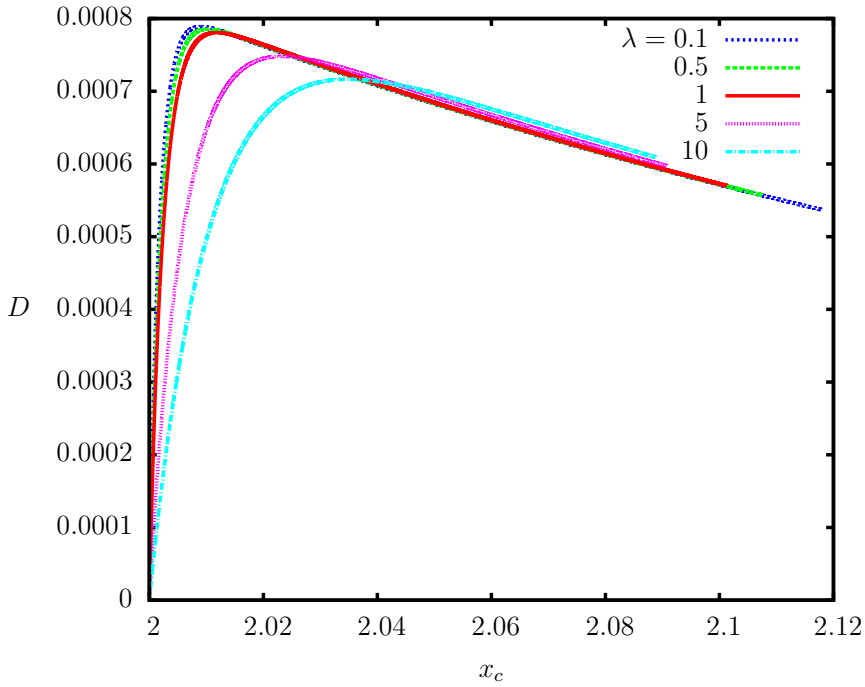

Figure 53. Droplet deformation D as a function of location x_c under the influence of λ when $Q = 0.8$, $L = 2$ and $Ca_E = 0.2$ for a perfect dielectric system.

The droplet deformation D decreases with the viscosity ratio λ increasing in the perfect dielectric system. With larger λ value, the droplet has a slower response to the applied electric force, so a droplet with a larger value in λ generally exhibits a smaller deformation D. In Fig. 53, when the droplet moves away from the point charge, the droplet deforms rapidly at the beginning. After the deformation D reaches the maximum, the value of D starts to decrease slowly. The initial increase in D is slower for larger λ. The droplet deformation shows a monotonic decrease as λ increases for a droplet moves towards the point charge as shown in Fig. 54. This behavior is similar to what happens in a leaky dielectric system (Fig. 38).

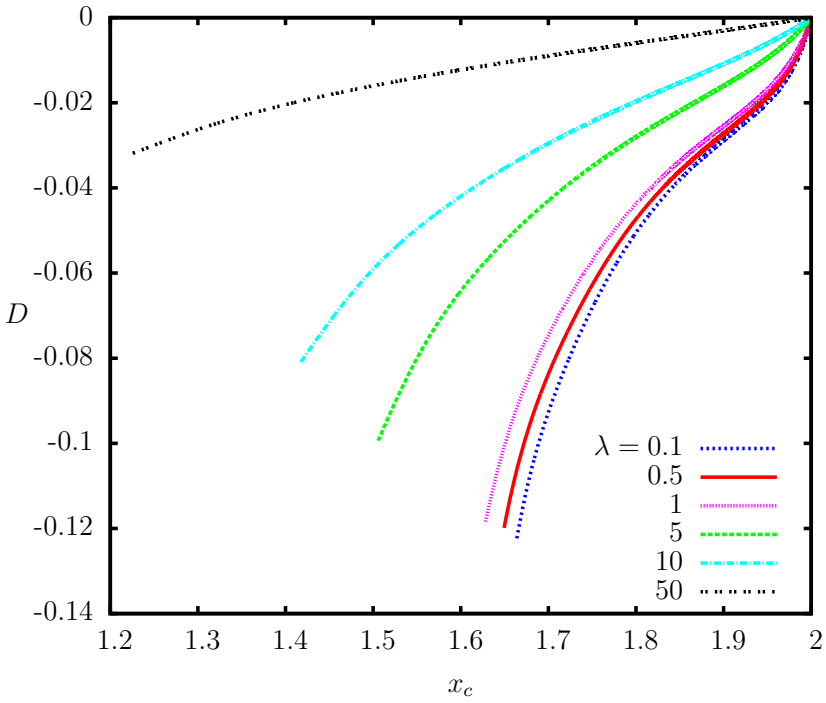

Figure 54. Droplet deformation D as a function of location x_c under the influence of λ when $Q = 10$, $L = 2$ and $Ca_E = 0.2$ for a perfect dielectric system.

CHAPTER 7. CONCLUSIONS AND FUTURE WORK

In this study, we successfully modified and employed a three-dimensional spectral boundary element method for the droplet behavior in a steady electric field. This method is validated by comparing others' computational results and our experimental results. We investigated the deformation and migration of a droplet for both a leaky dielectric system and a perfect dielectric system in a steady non-uniform electric field created by a point charge.

We found that when neither resistivity ratio R nor permittivity ratio Q equals to 1, the droplet migrate either in the direction of the point charge or away from the point charge. If it is a leaky dielectric system the resistivity ratio R determines droplet migration direction. If $R > 1$ (the droplet is less conductive than the suspending fluid), the droplet is found to move to the weaker electric field. The droplet may migrate towards the point charge if $R < 1$. When $R = 1$, the droplet moves to the stronger electric field if $Q > 1$ (the droplet is more polarizable than the surrounding fluid). The droplet may move to the weaker electric field if $Q < 1$. The droplet migration velocity u_x generally tends to decrease if the droplet moves to the weaker electric field, while u_x increases if the droplet moves to the point charge. In addition, the droplet speed always increases with Q increasing. In the leaky dielectric system, the droplet may get more deformation with a larger R or Q value when the droplet moves to the weaker electric field. But if the droplet moves to the stronger electric field, the droplet deformation shows a complicated behavior in response to R and Q. The droplet may deform into distinctive shapes (with a sharp tip or a dimple) depending on the value of R and Q in the $R - Q$ diagram.

In the perfect dielectric system, R does not have an influence on the droplet behavior. Permittivity ratio Q decides which direction the droplet moves to and what deformation shape the droplet may have. When $Q > 1$, the droplet moves to the stronger electric field and the deformation becomes $D < 0$. The droplet migrates towards weaker electric field and the deformation becomes $D > 0$ when $Q < 1$. A larger difference of the droplet permittivity

and the surrounding liquid permittivity could increase the droplet migration speed and the deformation in the perfect dielectric system. We also find the droplet moves faster for the perfect dielectric system than for the leaky dielectric system.

For both leaky dielectric system and perfect dielectric system, the electric capillary number Ca_E and the viscosity ratio λ could not alter the droplet migration direction or determine the droplet shape. However, these two parameters affect the droplet velocity and deformation magnitude. When a larger Ca_E value supplies a larger electrical force on the droplet, it increases the droplet velocity and the deformation. A larger λ hinders the droplet movement, reduces the droplet velocity, and at the same time incurs a smaller deformation. The effect of Ca_E and λ on the droplet deformation and velocity is more substantial for the perfect dielectric system than for the leaky dielectric system.

There are several innovations in this study. Firstly, we are the first one to use the three-dimensional spectral boundary element method to solve a droplet migration and deformation problem under a non-uniform electric field. Secondly, the non-uniform electric field in our research was supplied by a point charge. This kind of electric field is the fundamental of the co-planer plate electrodes that have more real applications and could be set up in future experiments and industry. In the future, we will investigate the droplet migration in microfluidic channels mounted with co-planar plate electrodes. Thirdly, this study reveals how the relative permittivity and conductivity, the electric capillary number and the viscosity ratio influence droplets migration and deformation in a non-uniform electric field. We listed the critical values of R and Q for the droplet migration direction. These values could be used in the future research and industry application for the liquid-liquid dispersion system. This thesis provides reference for the future theoretical and computational investigations on droplet motion in digital microfluids under the different types of non-uniform electric fields.

REFERENCES

[1] O. O. Ajayi, *A note on taylor's electrohydrodynamic theory*, Mathematical and Physical Sciences **364** (1978), 499–507.

[2] R. S. Allen and S. G. Mason, *Particle behaviour in shear and electric fields. I: Deformation and burst of fluid drops.*, Proc. R. Soc. Lond. A **267** (1962), 45–61.

[3] E. Baird, P. Young, and K. Mohseni, *Electrostatic force calculation for an ewod-actuated droplet*, Microfluid Nanofluid **3** (2007), 635–644.

[4] J. C. Baygents, N. J. Rivette, and H. A. Stone, *Electrohydrodynamic deformation and interaction of drop pairs*, J. Fluid Mech. **368** (1998), 359–375.

[5] C. H. Byers, *Understand the potential of electro-separations.*, Chem. Eng. Prog. **91** (1995), 63–69.

[6] J. S. Crane and H. A. Pohl, *Theoretical models of cellular dielectrophoresis*, Journal of Theoretical Biology **37** (1971), 15–41.

[7] S. D. Deshmukh and R. M. Thaokar, *Deformation, breakup and motion of a perfect dielectric drop in a quadrupole electric field*, Phys. of Fluid **24** (2012), 032105.

[8] P. Dimitrakopoulos and J. J. L. Higdon, *On the displacement of three-dimensional fluid droplets from solid surface in low-Reynolds-number shear flows*, J. Fluid Mech. **377** (1998), 189–222.

[9] N. Dubash and A. J. Mestel, *Behaviour of a conducting drop in a highly viscous fluid subject to an electric field*, J. Fluid Mech. **581** (2007), 469–493.

[10] J. Q. Feng, *Dielectrophoresis of a deformable fluid particle in a nonuniform electric field*, Phys. Rev. E **54** (1996), 4438–4441.

[11] J. Q. Feng and T. C. Scott, *A computational analysis of electrohydrodynamics of a leaky dielectric drop in an electric field*, J. Fluid Mech. **311** (1996), 289–326.

[12] A. Fernandez, *Response of an emulsion of leaky dielectric drops immersed in a simple shear flow: Drops less conductive than the suspending fluid*, Phys. Fluids **20** (2008), 043304.

[13] A. Fernandez and G. Tryggvason, *The effects of electrostatic forces on the distribution of drops in a channel flow: two-dimensional oblate drops*, Phys. Fluids **17** (2005), 093302.

[14] J. Ha and S. Yang, *Deformation and breakup of newtonian and non-newtonian conducting drops in an electric field*, J. Fluid Mech. **405** (2000), 131–156.

[15] J. Hua, L. K. Lim, and C. H. Wang, *Numerical simulation of deformation/motion of a drop suspended in viscous liquids under influence of steady electric fields*, Phys. Fluids **20** (2008), 113302.

[16] J. D. Zahn J. Zhang and H. Lin, *A transient solution for droplet deformation under electric fields.*, Physics of Fluids **131** (2012), 12107878.

[17] E. Lac and G. M. Homsy, *Axisymmetric deformation and stability of a viscous drop in a steady electric field*, J. Fluid Mech. **590** (2007), 239–264.

[18] J. R. Melcher and G. I. Taylor, *Electrohydrodynamics: a review of the role of interfactial shear stresses*, Annu. Rev. Fluid Mech. **1** (1969), 111–146.

[19] M. Miksis, *Shape of a drop in an electric field*, Phys. Fluids **11** (1981), 1967–1972.

[20] G. P. Muldowner and J. J. L. Higdon, *A spectral boundary element approach to three dimensional stokes flow.*, J. Fluid Mech. **298** (1995), 193.

[21] C. T. O'Konski and H. C. Thacher, *The distortion of aerosol droplets by an electric field*, J. Phys. Chem. **57** (1953), 955–958.

[22] C. Pozrikidis, *Boundary integral and singularity methods for linearized viscous flow*, Cambridge University Press, New York, NY, 1992.

[23] D. A. Saville, *Electrohydrodynamics: the taylor-melcher leaky dielectric model*, Annu. Rev. Fluid Mech. **29** (1997), 27–64.

[24] J. D. Sherwood, *The deformation of a fluid drop in an electric field: a slender-body analysis*, J. Phys. A: Math. Gen. **24** (1991), 4047–4053.

[25] P. Singh and N. Aubry, *Transport and deformation of droplets in a microdevice using dielectrophoresis*, Electrophoresis **28** (2007), 644–657.

[26] G. Supeene, C. R. Koch, and S. Bhattacharjee, *Deformation of a droplet in an electric field: nonlinear transient response in perfect and leaky dielectric media*, Journal of Colloid and Interface Sience **318** (2008), 463–476.

[27] M. Sussman and E. G. Puckett, *A coupled level set and volume-of-fluid method for computing 3D and axisymmetric incompressible two phase flows*, J. Comput. Phys. **114** (2000), 146–159.

[28] G. Taylor, *Disintegration of water drops in an electric field*, Mathematical and Physical Sciences **280** (1964), 383–397.

[29] G. I. Taylor, *The formation of emulsion in definable fields of flow.*, P. Royal Society **146** (1934), 19340169.

[30] K. E. Teigen and S. T. Munkejord, *Sharp interface simulations of surfactant-covered drops in electric field*, (2010).

[31] R. M. Thaokar, *Dielectrophoresis and deformation of a liquid drop in a non-uniform , axisymmetric ac electric field*, European Physical Journal E **35** (2012), 76.

[32] S. Torza, R. G. Cox, and S. G. Mason, *Electrohydrodynamic deformation and burst of liquid drops*, Phil. Trans. R. Soc. Land A **269** (1971), 295–319.

[33] S. O. Unverdi and G. Tryggvason, *A front-tracking method for viscous, incompressible, multi-fluid flows*, Journal of Computational Physics **100** (1992), 25–37.

[34] O. Vizika and D. A. Saville, *The electrohydrodynamic deformation of drops suspended in liquids in steady and oscillatory electric fields*, J. Fluid Mech. **239** (1992), 1–21.

[35] Y. Wang and P. Dimitrakopoulos, *A three-dimensional spectral boundary element algorithm for interfacial dynamics in Stokes flow*, Phys. Fluids **18** (2006), 082106.

[36] X. Xu and G. M. Homsy, *The settling velocity and shape distortion of drops in a uniform electric field*, J. Fluid Mech. **564** (2006), 395–414.

[37] J. Zhang and D.Y. Kwok, *A 2D lattice boltzmann study on electrohydrodynamic drop deformation with the leaky dielectric theory*, J. Comput. Phys. **206** (2005), 150–161.